A Seabased Wave Energy Device:

An Experimental Investigation

A thesis

submitted in fulfilment

of the requirements for the degree

of

Master of Engineering

At

The University of Waikato

by

HAOFENG ZHU

THE UNIVERSITY OF
WAIKATO
Te Whare Wānanga o Waikato

2020

Abstract

Ocean waves are a largely untapped treasure-house of renewable energy resource, and the potential renewable energy harvested from ocean waves is considerable around the world. Abundant research and development on this field have been conducted to accomplish the aims in different stages, and the technology has been undergoing all the time. However, despite tremendous energy potential, technologies of ocean wave, the wave energy converter (WEC), are still relatively immature compared to other renewable technologies.

This thesis presents basic motion character of a WEC device that the performance of one of WECs in relationship between power take off (PTO) part and buoy. The device is a simple 1:50 scaled model which referred to a point absorber buoy device like the device of the Seabased project that the buoy connected with PTO by a wire reacts the water surface to respond excited waves, and drives the PTO with a spring.

The tests were conducted in a small water tank. In order to investigate the relationship between buoy performance and PTO part, two different springs were used respectively in PTO, which one spring is stiff and the other one is softer, and model device experienced irregular and regular wave conditions. The softer spring case indicated that the buoy was sensitive to the passing waves but it was hard to provide a restoring force, so the period of one heave motion of buoy was relatively long, which was totally opposed to that of the stiffer spring case. Moreover, the natural frequency of model device was also calculated by mathematical model, and this theoretical value was less than that of experimental value from test.

This model device could be improved and perfected and subjected to small scaled water tank tests for offshore device to investigate the basic characters for motion with methods of mathematical model or simulation and experimental results.

Preface and Acknowledgements

This is my first time to do an individual research. Although the journey to finish was full of hardships and frustrations, it was finally accomplished with my perseverance and most important support of my supervisor, a PhD student, all technicians, friends and my parents.

First of foremost, I would like to express my deepest gratitude and respect to my supervisor, Dr Martin J. Atkins, for his patiently continued guidance and support.

With the guidance of Dr Martin, I always got out of theory and practice stuck, and enhanced my knowledge. Without Dr Martin, I could have done the research and thesis.

I would like to thank the PhD student, Danielle Bertram, for her patience, guidance and encouragement. Danielle always shared her research experience and method, and made me take progress of the research all the time.

To all technicians, especially Ben Mcguinness, Jack Hies, and Jonathan van Harselaar who helped with design and improvement of model device in the lab.

Eventually, thanks to my parents who have given me everything.

Table of Contents

List of Figures

List of Tables

Nomenclature

Acronyms

AWS	Archimedes Wave Swing
BBDB	Backward Bent Duct Buoy
EMEC	European Marine Energy Centre
OTEC	Ocean Thermal Energy Conversion
OWC	Oscillation Water Column
RAO	Response Amplitude Operator
SSG	Seawave Slot-Cone Generator
TAPCHAN	Tapered Channel Wave Power Device
WEC	Wave energy converter

Symbols

A	Section area of buoy (m^2)
c	Damping coefficient (N·s/m)
c_c	Critical damping (N·s/m)
d	Diameter of buoy (m)
f	Wave frequency (Hz)
f_0	Natural Frequency of device (Hz)
F_C	Damping force (N)
F_E	External force (N)
F_K	Spring force (N)
g	Gravity acceleration (m/s^2)
H	Wave height (m)

J	Power flux (kW/m of wave crest)
k	Constant of spring under hydrostatic buoyancy condition
k	Wave number
KPTO	Stiffness of PTO, the spring constant (N/m)
L	Height of buoy (m)
M	Added mass (kg)
m	Mass of buoy (kg)
m	Mass of buoy or the total mass of buoy and ballast (kg)
T	Wave period (s)
δ	Logarithmic decrement
ζ	Damping ratio
λ	Wavelength (m)
ρ	Water density (kg/m^3)
ω	Angular frequency (rad/s)
ω_d	Frequency of damped vibration (rad/s)
ω_n	Circular natural frequency (rad/s)
ω_n	Circular natural frequency (rad/s)

1. Introduction

1.1. Context

Sustainable development and environmental protection have been being followed with interest all the time, and have resulted in a critical demand for generation of cleaner energy technologies. As is well known, more than 83% of the global primary energy (Greaves & Iglesias, 2018) are derived from fossil fuels, mainly coal, oil and natural gas. In terms of global electricity generation only 26.2%, including 15.8% hydropower, was from renewable energy sources in 2018, (Murdock et al., 2019). Thus, it can be seen that the fossil fuels are still the predominant source for energy production and electricity generation.

A major issue with the use of fossil fuels is that they produce a large number of greenhouse gas emissions, which leads to serious impact on the global environment and climate change. Thereby it is imperative to focus on exploring alternative and renewable sources to generate electricity and decrease the generation of carbon and greenhouse gas emissions. Actually, this issue has been a concern since the late 1990s (Greaves & Iglesias, 2018; Li & Yu, 2012), and different types of renewable energy technologies have been developing to help provide clean solutions. Renewable electricity generation methods including solar, wind and hydropower are mature technologies and, in some cases, can compete or outdo conventional fossil fuel-based methods in cost.

Wave energy is an alternative renewable energy resource, although it is currently underutilized due to a lack of technically mature or economically viable methods to exploit it (Kelly, Dooley, Campbell, & Ringwood, 2013). Wave energy has a tremendous potential, estimated to have between 8,000 and 80,000 TW for annual generation potential globally (Xie & Zuo, 2013).

As research and development of wave energy technologies growing rapidly, a

variety of Wave Energy Converters (WECs) have been investigated or are under development, and different solutions and patents have been constructed in relevant location according to wave regimes, the sea state and energy density. For example, the Seabased Project (Hong, 2016) is one of representative wave energy projects, led by Uppsala University, Sweden. This project started in 2002, and composed various WECs which have been deployed and researched since 2006. Currently a pilot installation has been constructed and operational since 2006 off the west coast of Sweden and a 100 MW wave Power Park has been contracted in Ghana in 2018.

Other oceanic countries like the United States, the United Kingdom, Denmark, Ireland, and Portugal and so on, have been developing their projects respectively. Moreover, some international organizations, for instance, the International Energy Agency and the International Electrotechnical Commission, are also working on design and test wave energy devices (Li & Yu, 2012).

1.2. Benefits and challenges

As with all new and developing technology there are both benefits and challenges and wave energy is no exception. These are outlined below

Benefits

- Wave energy offers the highest energy density compared with other major renewable energy sources such as wind and solar (Czech & Bauer, 2012; Drew, Plummer, & Sahinkaya, 2009).
- Compared with other renewable energy sources, wave energy has limited negative environmental impact (Czech & Bauer, 2012; Drew et al., 2009).
- Waves can travel large distances with a less energy loss than other green energy, which is a unique character of wave energy (Czech & Bauer, 2012; Drew et al., 2009).

- WECs are able to produce power up to 90% of the time which is much higher than that of wind and solar power devices, typically at only 20% to 30% (Pelc & Fujita, 2002).
- The seasonal variability of the wave energy matches will the seasonal variation of energy demand (Drew et al., 2009).

Challenges

- A major challenge is the conversion of the slow (-0.1 Hz), irregular and intensive oscillatory motion to drive a generator with output quality acceptable to the utility network (Czech & Bauer, 2012; Drew et al., 2009).
- WEC have to be tuned to the wave resource in order to get high operational efficiency because of the various factors of the wave including wave height, phase and direction (Czech & Bauer, 2012).
- To capture wave power under irregular wave environment conditions and to withstand extreme wave conditions. These influence the design of WEC devices. Additionally, extreme environment lead to severe challenges of construction and capital costs (Drew et al., 2009).
- The devices have to be operated under the highly corrosive environment (Drew et al., 2009).

1.3. Thesis Aim

The aim of this thesis is to test a simple 1:50 point absorber buoy device. The detailed tests are to investigate the relationship between buoy performance and power take-off unit with two different constant springs under regular and irregular wave conditions. The Response Amplitude Operators (RAO) will be calculated.

1.4. Thesis Outline

Chapter 2 introduces the ocean energy forms and the characteristics of waves. The classification of wave energy converters and working principle as well as a brief history on wave energy development also reviewed. Moreover, some specific WECs are introduced, especially the point absorber, and the wave resource assessment is also presented.

Chapter 3 presents the description of the device design and experiment set up with test aims and procedures. This chapter also describes the mathematical model of device and method of experimental results analysis. The RAO developed and analysis method are presented.

Chapter 4 contains the results of the experiment work and discusses the results. A wave resource assessment for two sites off the coast of New Zealand are presented using 20 years of wave data to provide some detail on the power density of full-scale projects.

Chapter 5 presents the conclusions from the work and makes recommendations for future work.

2. Literature Review

2.1. Ocean Energy

Oceans cover more than 70% surface area of the earth and contain several potential renewable energy sources. These come in a variety of energy types such as kinetic, heat and chemical energy (Grabbe, Lundin, & Leijon, 2001). Ocean energy can be harnessed from six sources which are wave energy, tidal range, tidal currents, ocean currents, ocean thermal energy conversion, and salinity gradients (Edenhofer et al., 2011). Figure 1 shows the distribution of some ocean energy in the world.

Wave energy

Wave energy is transferred from the wind blowing over the surface of ocean. As a high efficiency of energy transformation, waves can travel long distances, and abundant wave energy is distributed between 30° and 60° of north and south latitudes. Theoretically, it contains 32,000 TWh/yr, but some of this energy cannot be harvested due to the restriction of wave energy technology currently developed (Edenhofer et al., 2011).

Tidal range

Tidal range is the rising and falling of tides which are cause by gravitational, rotational, and other acting forces of the Earth-Moon-Sun system. It can be predicted, and most coastal areas usually occur two high and low tides in every single day. The energy of tide range distributes in relatively shallow water area, with the theoretically potential power of between 1 to 3 TW (Edenhofer et al., 2011).

Tidal currents

Tidal currents come from horizontal motion of water flows which are cause by rise

and fall of the tides (Edenhofer et al., 2011). The potential tidal current generation capacity is estimated to exceed 120 GW internationally (MarineEnergy, 2020)

Ocean currents

Ocean currents derive from wind-driven and thermohaline circulations which exist in the open ocean. The currents flow keeps the same propagation directions with slight variation (Edenhofer et al., 2011).

Ocean thermal energy conversion (OTEC)

Ocean thermal energy are produced by roughly 15% of the solar input, and these thermal energies can be reserved from the upper ocean layer to deep cold ocean (1,000 m depth), with the exponential decrease by depth due to the low thermal conductivity of seawater. Despite the low density of OTEC, it is considered an enormous source which is much larger than other sources, with the estimated amount, 44,000 TWh/yr (Edenhofer et al., 2011).

Salinity gradients

Salinity gradients are generated by the pressure from different salinity of freshwater and seawater with passing a semi-permeable membrane. It is also osmotic power which can be produced in a sufficient freshwater place, like river mouths which is the junction of freshwater and seawater. The energy potential of salinity gradients is estimated to be 1,650 TWh/yr (Edenhofer et al., 2011).

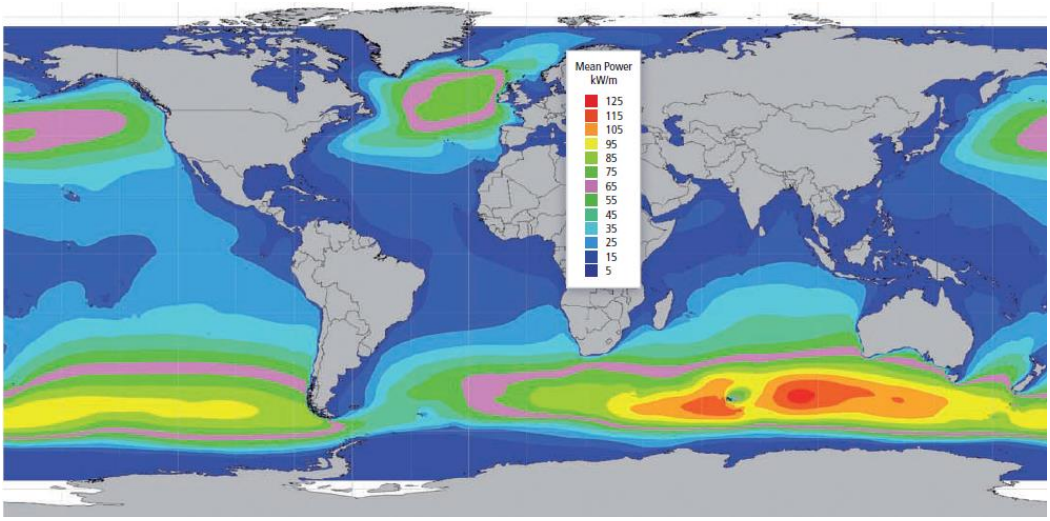

(a)

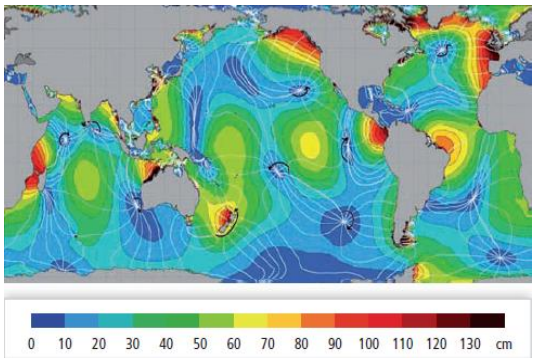

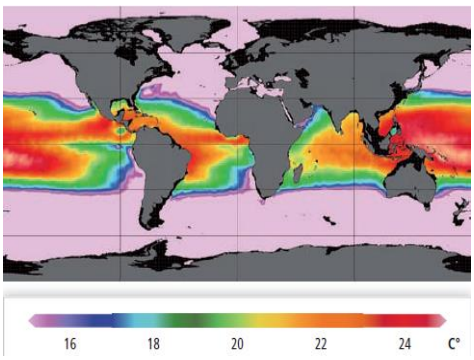

(b) **(c)**

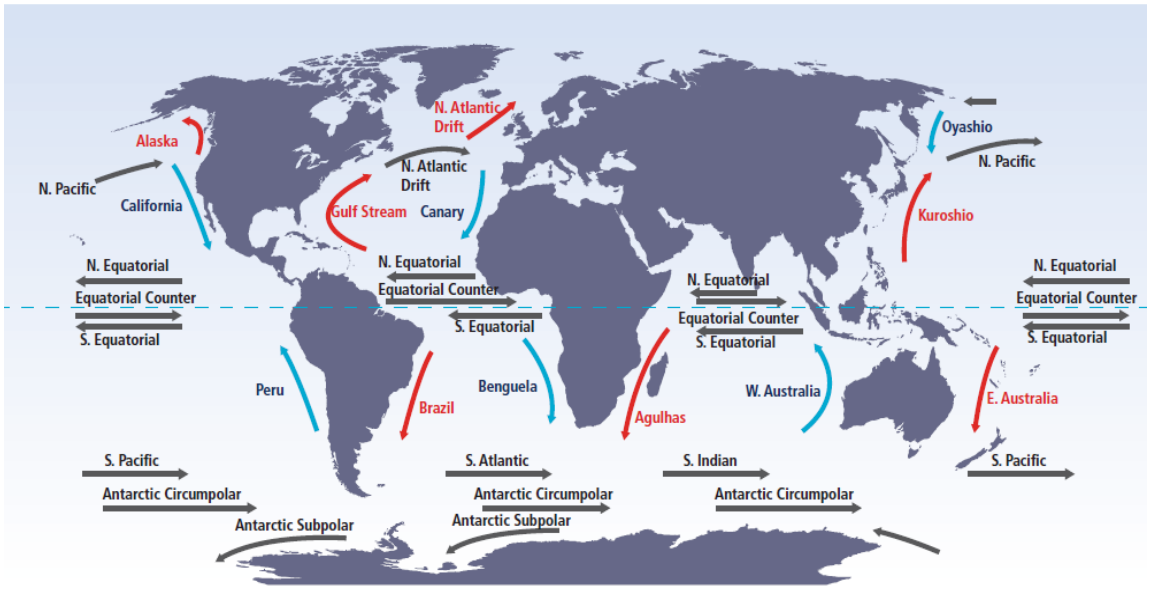

(d)

Figure 1. Distribution of some ocean sources (a) wave source; (b) Tidal range; (c) Ocean thermal energy; and (d) Ocean currents (Edenhofer et al., 2011).

2.2. Ocean waves

All waves are generated by disturbances, which is derived energy movement transmitting through different medium e.g. solid, liquid, or gas. The energy movement is apparent in ocean waves by rising and falling motion on the surface of ocean waves (Garrison, 2012).

2.3. Ocean wave formation

Ocean waves can be classified into various types with three basic influence factors – disturbing force, restoring force, and wavelength.

The formation of ocean waves is caused by disturbing forces with different energy sources. These sources of energy may come from meteorological factors such as wind and changes in atmospheric pressure, or geological activities, such as earthquakes and volcano eruption. According to these energy sources and intensity, the types of ocean waves primarily contain capillary wave, wind wave, seiche, tsunami and tide. Once the ocean waves are formed, the restoring force as a dominant force is to make the surface of waves to be flatness. Wavelength is used to measure wave size which is the horizontal distance of two successive crests or troughs. Table 1 illustrates the characteristics of wave types, and Figure 2 shows the relationships of these characteristics with amount of energy and period for each wave type (Garrison, 2012).

Table 1. Disturbing, restoring force and wavelength for each wave types (Garrison, 2012).

Disturbing Forces, Wavelength, and Restoring Forces of Ocean Waves			
Wave Type	**Disturbing Force**	**Restoring Force**	**Typical Wavelength**
Capillary wave	Usually wind	Cohesion of water molecules	Up to 1.73 cm (0.68 in)
Wind wave	Wind over ocean	Gravity	60-150 m (200-500 ft)
Seiche	Change in atmospheric pressure, storm surge, tsunami	Gravity	Large, variable; a function of ocean basin size
Seismic sea wave	Faulting of seafloor, volcanic eruption, landslide	Gravity	200 km
Tide	Gravitational attraction, rotation of Earth	Gravity	Half Earth's circumference

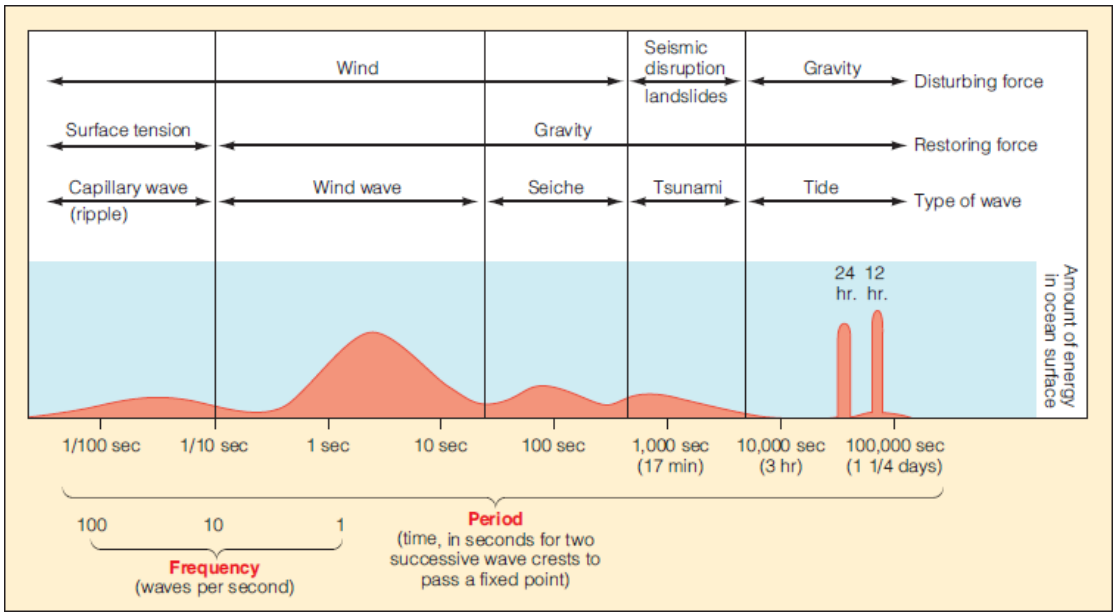

Figure 2. Relationships of disturbing and restoring force with amount of energy and period for different wave types (Garrison, 2012).

2.4. Definition and symbols of wave

A basic wave can be described as a sinusoidal variation (Pecher, Kofoed, & SpringerLink, 2017), using right-handed, Cartesian coordinate system (Salmon, 2008) as in Figure 3. Definition and symbols of a sinusoidal wave (Pecher et al., 2017)., where *a* is the wave amplitude, *H* is the wave height, *T* is the wave period, λ is the wave length. The basic wave parameters are summarised in Table 2.

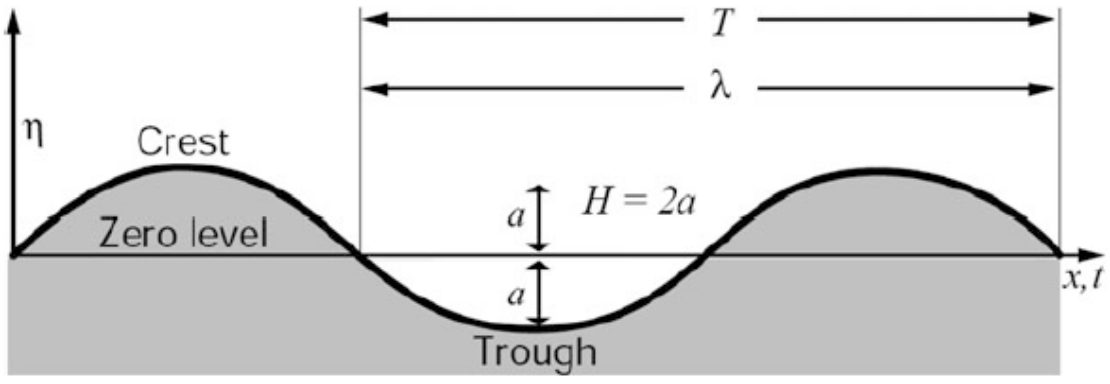

Figure 3. Definition and symbols of a sinusoidal wave (Pecher et al., 2017).

Table 2. Basic wave parameter and definitions.

Parameter	**Definition**
Wave crest	the height part of the wave above average water level
Wave trough	the valley between wave crests below average water level
Wave height (H)	the vertical distance between a wave crest and the adjacent trough
Wave length (λ)	the horizontal distance between two successive crests or trough
Wave period (T)	the time taking for a wave to move a distance of one wavelength
Wave frequency (f)	the number of waves passing a fixed point per second $$\mathrm{f} = \frac{1}{T}$$
Angular frequency (ω)	$$\omega = \frac{2\pi}{T} = 2\pi f$$
Wave number	$$\mathrm{k} = \frac{2\pi}{T}$$

Wind waves

The energy which is captured by WECs are derived from surface waves that are usually generated by wind. These are known as wind waves (Pecher et al., 2017). The formation of wind waves is relatively slow, forming over time in an area called the fetch as in Figure 4 (Lynn, 2014). Wind constantly transfers energy to produce small ripples on the surface of sea with the size increasing due to the sustained energy from wind, but the waves gradually achieve fully developed with no increase in size because of energy loss (Pecher et al., 2017). The waves will travel

long distances from deep water to form the swell waves with losing almost no energy. However, when waves approach the shoreline into shallow water area, waves get slow in speed and dissipate an amount of energy after breaking onshore (Lynn, 2014).

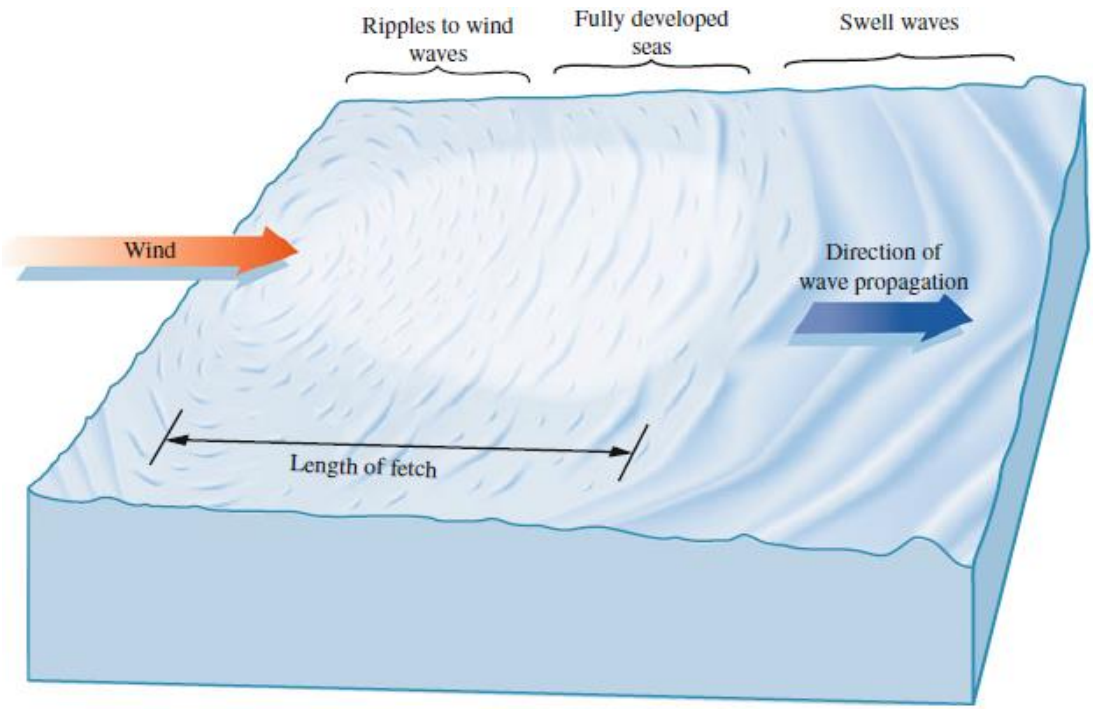

Figure 4. Formation of waves by wind (Garrison, 2012).

2.5. History of wave energy

The history of WECs can trace back to more than 200 years (Falcão, 2014; Greaves & Iglesias, 2018; Lynn, 2014). In 1799, the first WEC was patented by Monsieur Girard and his son in Paris (Falcão, 2014; Greaves & Iglesias, 2018; Lynn, 2014). From the end of 19th century to the early of 20th century, there are two historical designs should be mentioned. In 1898, the patent of the 'wave motor' shoreline system was granted to P. Wright in the USA, and by the 1910, one of earliest oscillating water column converter was able to generate up to 1 kW electricity which was created by Monsieur Bochaux-praceique in France (Lynn, 2014).

In the 20th century, Yoshio Masuda, a Japanese inventor, who is regarded as the

pioneer of the modern WEC, designed an oscillating water column power buoy which was commercialized in 1965 (Falcão, 2014; Greaves & Iglesias, 2018; Lynn, 2014). After that, the first oil crisis of the 1970s increased interest in the generation of renewable energy from waves (Falcão, 2014; Greaves & Iglesias, 2018; Lynn, 2014). With a paper, *Wave power* (Salter, 1974), published in Nature journal by Stephen Salter from the University of Edinburgh, it was a landmark to improve further the awareness of development of wave energy within the scientific community, motivating the UK and Norway consecutively to implement their own wave development programs (Falcão, 2014; Lynn, 2014). Although the support of wave energy development and research was reduced sharply especially in UK by the 1980s, and it was focused on again from the 1990s in Europe and worldwide (Greaves & Iglesias, 2018).

The industry of wave energy absorption is a considerably tough process of hydrodynamics (Falcão, 2014), and the technologies are still in the development or early commercialisation stages of development (Greaves & Iglesias, 2018). Wave energy contains large potential around the world, and a several of types WECs have been creating continuously with some of them reached the full-scale prototype stage, and additionally, a growing number of pilot projects are also built up in the test sites (Greaves & Iglesias, 2018).

2.6. Classification of wave energy converters

Wave energy can be captured by a variety of wave energy technologies with over one thousand devices patented in Europe, Japan and North America (Chen, Yu, Hu, Meng, & Wen, 2013; Drew et al., 2009). These technologies can be generally classified by different ways according to the location, working principle and directional dependence as in Figure 5 (Bull & Ochs, 2013).

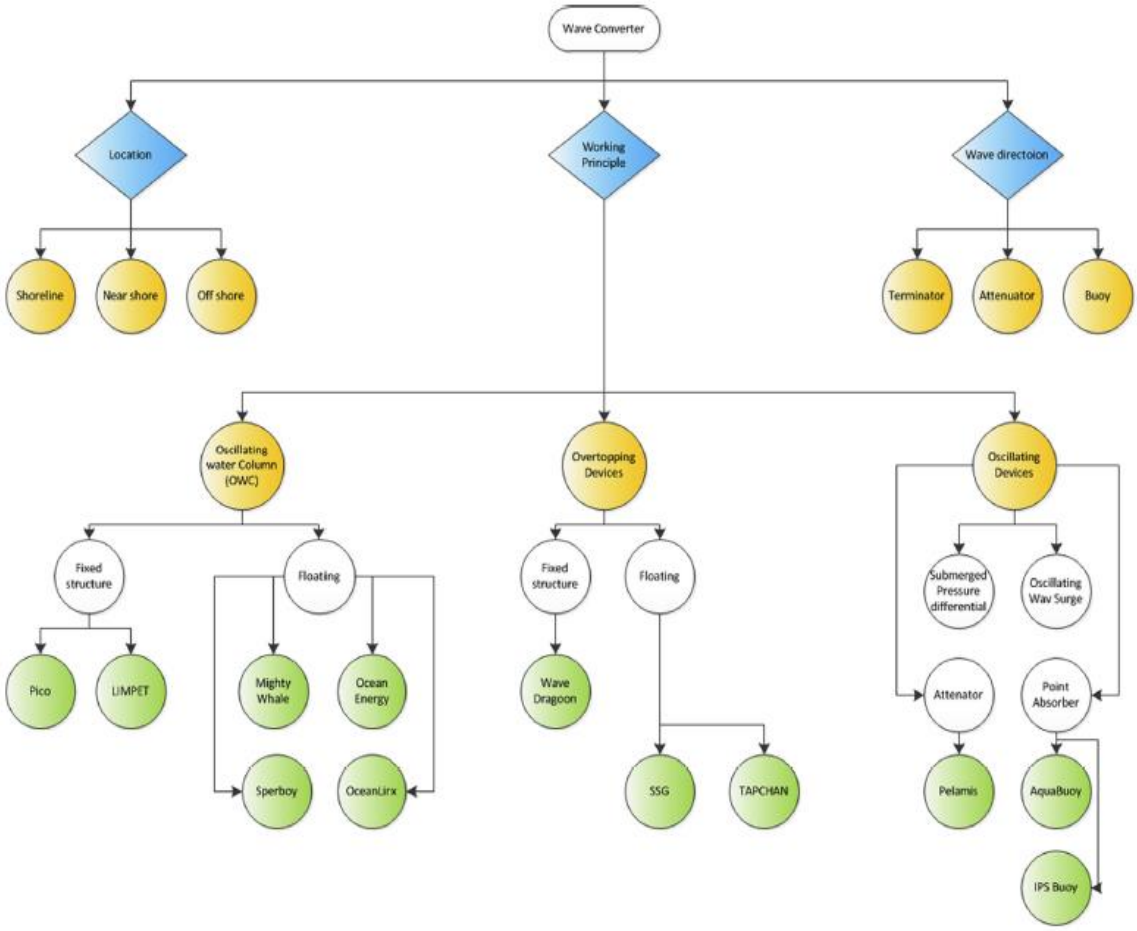

Figure 5. Classification of WECs (Fadaeenejad, Shamsipour, Rokni, & Gomes, 2014)

2.6.1. Location

Surface waves of oceans are generated by the wind (Lynn, 2014). Energy will be lost as surface waves move into shallow water as they approach the shore (Lynn, 2014). Based on this fact, the distance of the WEC from the shore determines the efficiency of technologies to absorb the energy of wave. Three classification of locations exist, shoreline, nearshore and offshore as in Figure 6 (Lynn, 2014).

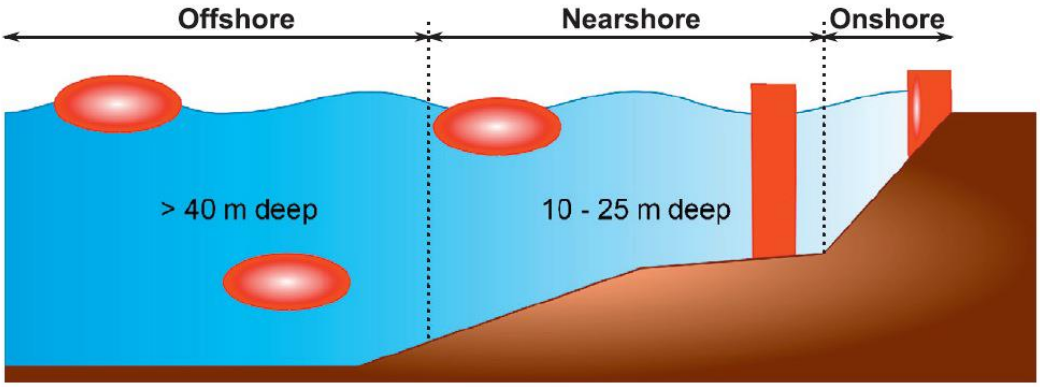

Figure 6. Location for WECs (Titah-Benbouzid & Benbouzid, 2015)

Shoreline devices

Shoreline WEC are installed or embedded on the land at the shoreline (Lynn, 2014; Poullikkas, 2014). The advantages of shoreline devices include: they are easy to construct (Drew et al., 2009) and maintain (Drew et al., 2009; Poullikkas, 2014) with no considerations of mooring or long electrical cable runs (Poullikkas, 2014). In addition, the damage of devices would be decreased probably due to the surface waves are moderated when they move into the shallow water (Drew et al., 2009). On the other hand, under similar conditions, shoreline systems will generate less energy due to the reduced power density around 20 kW/m compared to offshore systems at around 70 kW/m (Drew et al., 2009; Poullikkas, 2014). A number of other of considerations, such as location, topography and landforms, and coastal environmental protection, also restrict the development of shoreline systems and widespread application (Drew et al., 2009).

Nearshore devices

Nearshore WECs are those that are deployed in relatively shallow water, around 10 – 25 m in depth (Drew et al., 2009). Although there is no universally agreed upon definition on what “shallow” water means, it can refer to the depth of water less than a quarter wavelength (Drew et al., 2009). Nearshore devices are always constructed such that they are embedded or anchored to the seabed in some manner (Drew et al., 2009; Lynn, 2014; Poullikkas, 2014), and it may also be a

means of providing appropriate stability for devices to work (Drew et al., 2009).

The main drawback of nearshore systems is similar to the that of shoreline device in that they absorb much less energy due to the lower power density in the shallow water (Drew et al., 2009). Additionally, the nearshore systems are more prone to damage due to the unstable behaviour of shallow water waves (Poullikkas, 2014).

Offshore devices

The deployment of offshore WEC is usually in deep water. The deep water refers to the depth of water that is more than 40 m (Drew et al., 2009; Poullikkas, 2014). Offshore WECs are basically oscillating and floating bodies (Chen et al., 2013; Poullikkas, 2014), and are rarely fully submerged bodies (Poullikkas, 2014). The advantage of offshore systems is able to extract a greater amount of wave energy due to the high wave energy content in deep water (Chen et al., 2013; Drew et al., 2009; Poullikkas, 2014). However, the reality of the offshore environment leads to challenges in construction and maintenance. It is more difficult and higher cost to construct and maintain equipment in a marine environment due to factors such as sea conditions, the corrosive environment, large wave height, and wave energy content (Chen et al., 2013; Drew et al., 2009). In addition, these systems will be required to survive extreme weather events and wave conditions such as typhoons and hurricanes (Chen et al., 2013; Drew et al., 2009). These factor add significant additional cost to the design, construction and installation, operation and maintenance of offshore WEC installations (Drew et al., 2009).

2.6.2. Working principle

According to the working principle, WECs are classified into three types which are oscillation water column (OWC), oscillating bodies, overtopping as shown in Figure 7 (Falcão, 2014).

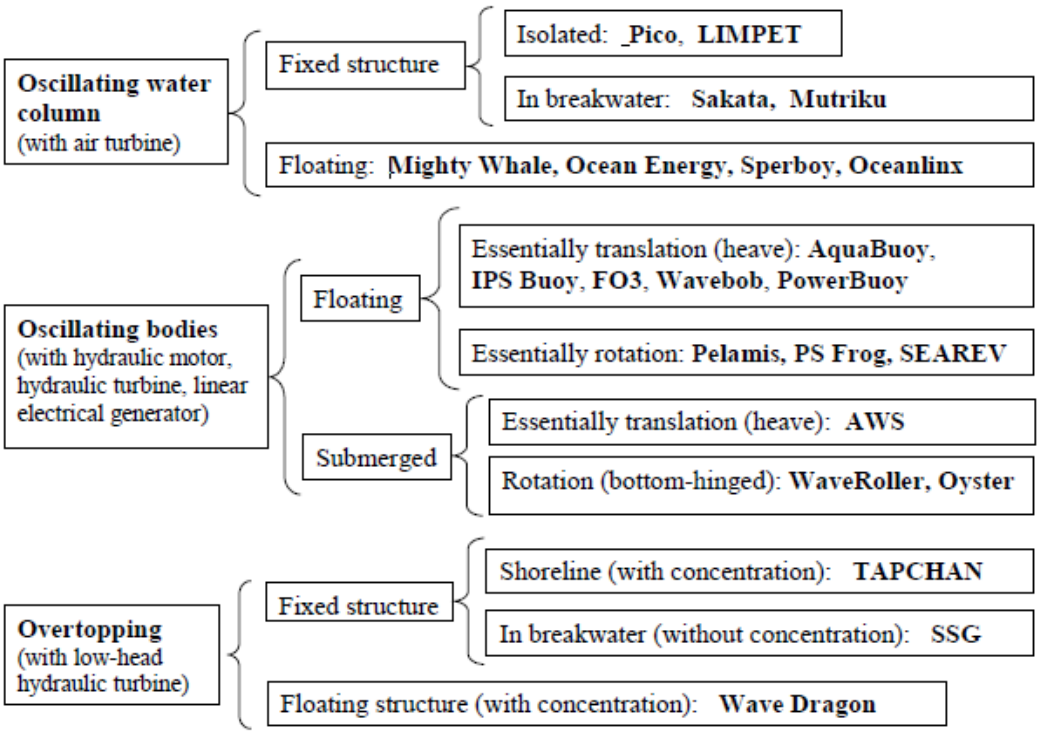

Figure 7. Classification of WECs according to working principle with examples of WEC included (Falcão, 2014).

Oscillating Water Columns

Oscillating water columns (OWC) are one of the most successful technologies in a variety of patented WECs all over the world due to the achieved in development of full-scaled prototypes (Greaves & Iglesias, 2018). For example, as the first large-scale type device, it was built up in Japan, in 1985 and India, in 1990 respectively (Greaves & Iglesias, 2018).

OWC technologies include two types of designs which are fixed-structure and floating-structure (Falcão, 2014; Greaves & Iglesias, 2018).

Fixed-structure devices, the shoreline device, are generally fixed to a seaside cliff or constructed on the bottom of sea, such as breakwater and sea wall structures (Falcão, 2014). Floating-structure devices locate in deep water which are also an offshore device, and they are usually floating freely under the wave motion in heave and pitch directions, for example, the Ocean Energy Buoy, backward bent duct buoy (BBDB), and the Mighty Whale (Greaves & Iglesias, 2018). OWCs devices

have a concrete or steel structure to form an air chamber which partly emerges in the seawater with opening below the surface of free water (Falcão, 2014). The water column of inner water surface oscillates the trapped air in the chamber so that the air is pushed to go through a turbine and drive it to convert wave energy into electricity (Falcão, 2014; Greaves & Iglesias, 2018). Some devices are shown in Figure 8.

As mentioned above, the location of fixed-structure OWCs devices is in the shallow water along the coast, so based on this fact, the advantages of fixed-structure OWCs devices are that these devices are able to work under a stable sea environment so that it makes devices be in long survivability (Greaves & Iglesias, 2018). Additionally, there is no requirements in mooring lines and cables compared to floating-structure devices. However, the drawback of fixed-structure OWCs are also obvious that there is about 70% loss in shallow water, and tidal range also impact the performance of these devices (Greaves & Iglesias, 2018). In the case of offshore floating-structure devices, these devices are established in deep water, so amount of energy can be converted from this area (Greaves & Iglesias, 2018). On the other hands, as a kind of offshore devices, the difficulties of these are mentioned in details in aspects of construction, maintenance and short service life.

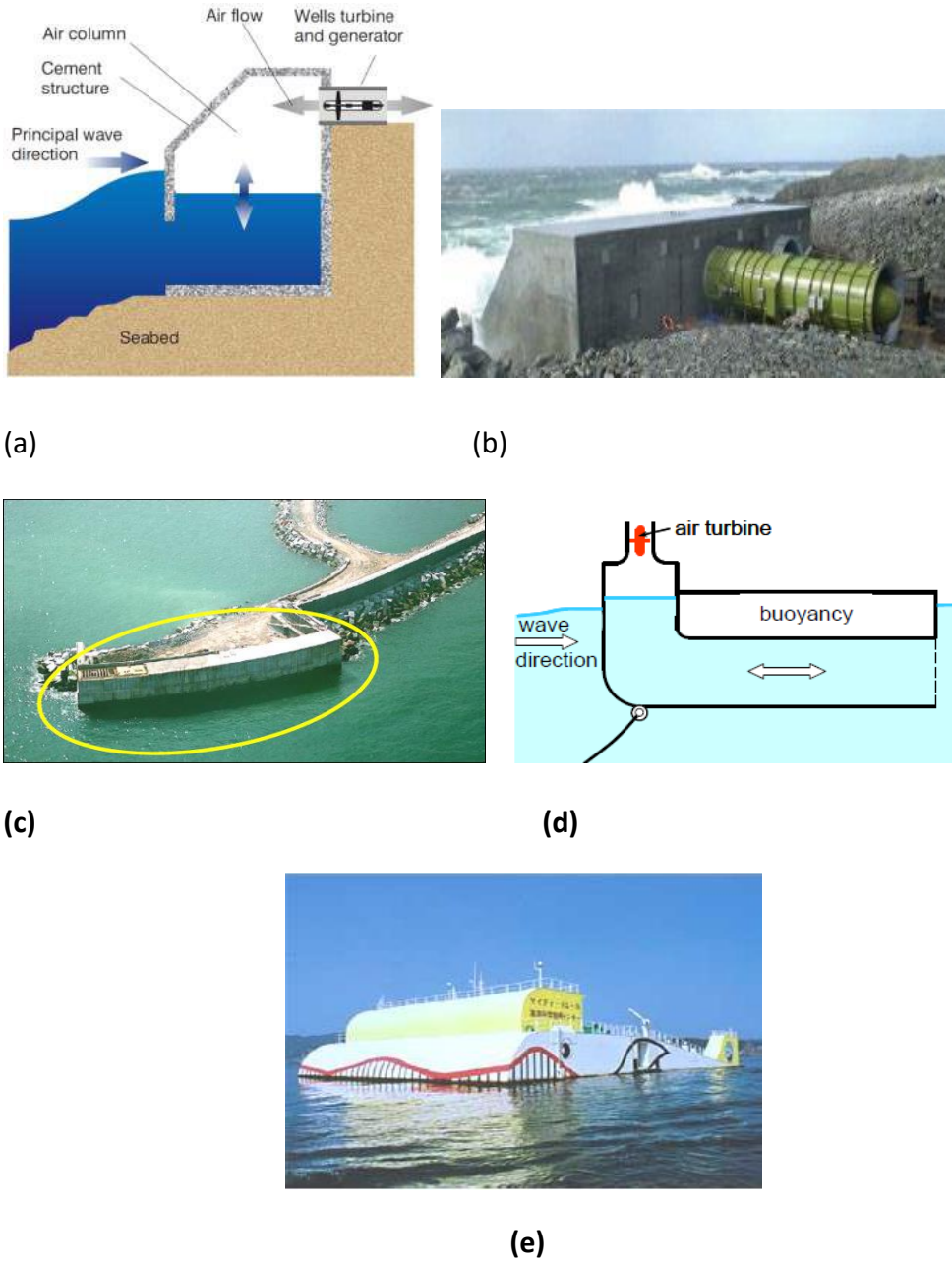

Figure 8. (a) Schematic of a fixed structure of OWC (Poullikkas, 2014), (b) LIMPET OWC plant (Falcão, 2014), (c) Mutriku breakwater (Falcão, 2014), (d) Schematic of BBDB (Falcão, 2014), (e) Mighty Whale (Falcão, 2014).

Oscillating Bodies

Oscillating bodies systems are offshore devices, and they are either floating or fully submerged in type (Falcão, 2014; Greaves & Iglesias, 2018). Single or multiple oscillating bodies are driven by the action of wave, and the motion of oscillators

are relative to the seabed or react against to oscillators themselves (Falcão, 2014; Greaves & Iglesias, 2018). By this way, wave energy can be extracted and converted into electricity by generators.

Fully submerged oscillating bodies less common than the floating type, but the Archimedes Wave Swing (AWS) is the typical one as illustrated in Figure 9 (Falcão, 2014; Greaves & Iglesias, 2018). The AWS device, which is a fully submerged oscillating body in heave to drive a linear electrical generator, was researched and developed in Holland, and the trial of devices was conducted in Portugal in 2004 (Falcão, 2014; Greaves & Iglesias, 2018).

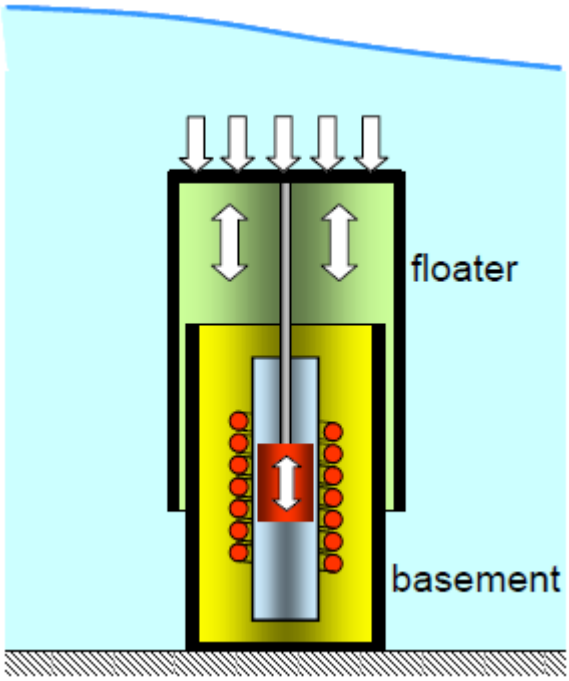

Figure 9. Schematic of the Archimedes Wave Swing (Falcão, 2014).

An example of floating devices, a seabed WEC was developed by Uppsala University, with a company Seabased (Poullikkas, 2014), which also uses a linear electrical generator connecting a taut-moored buoy located on the ocean floor as illustrated in Figure 10 (Falcão, 2014; Greaves & Iglesias, 2018).

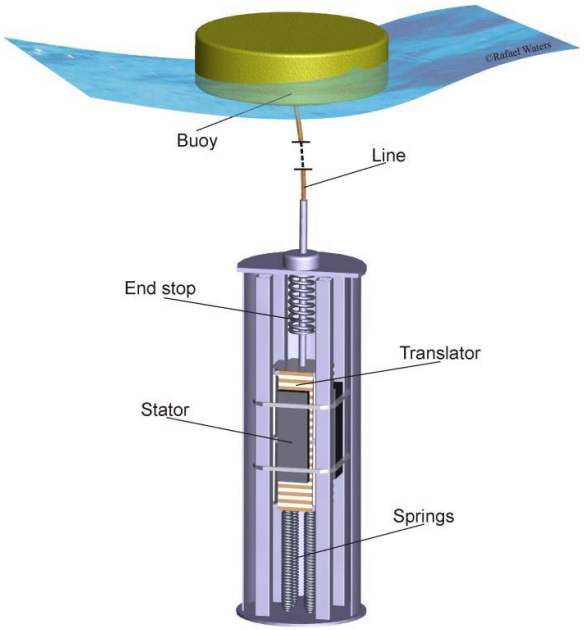

Figure 10. The Seabased WEC (Falcão, 2014).

An example of multiple oscillating bodies is the Pelamis consisting of a snake-shaped floating, multibody, pitching and yawning device with four oscillators, which are cylindrical sections connected by hinged joints. The Pelamis was developed in the UK in 2004 (Falcão, 2014), and further tested in Portugal in 2008 and the European Marine Energy Centre, EMEC, in 2010 to 2014 (Falcão, 2014; Greaves & Iglesias, 2018). Figure 11 shows the Pelamis device.

Figure 11. Pelamis wave farm (Drew et al., 2009).

Overtopping Systems

Overtopping systems use a different method to convert energy to electricity (Falcão, 2014). The seawater from incident waves is captured into a reservoir, which is higher than the average free-surface sea level of the surrounding sea, by over spilling of sea crest. The trapped seawater in the reservoir with potential energy pass through low-head turbines and flow back to sea (Greaves & Iglesias, 2018).

Overtopping devices are able to be deployed in different locations, which are shoreline and offshore. The TAPCHAN (Tapered Channel Wave Power Device) is an early case of a shoreline overtopping device, which was developed in Norway in the 1980s, and built at Toftestallen in Norway in 1985.

Offshore floating overtopping systems, are located offshore and operate on similar principles as shoreline devices. The Wave Dragon, developed in Demark in 2003 (Falcão, 2014; Greaves & Iglesias, 2018) is representative of such systems.

Overtopping systems can have a concentrator as part of the design that is able to concentrate the waves before they flow into the converter and a narrowing channel. By this way, it is helpful for systems to increase wave heights for water to fill up the reservoir by increasing the overtopping volume (Falcão, 2014). Both of the TAPCHAN and the Wave Dragon devices are designed with a concentrator (Greaves & Iglesias, 2018). By contrast, the Seawave Slot-Cone Generator (SSG) is an example of shoreline devices without any concentration (Greaves & Iglesias, 2018). Figure 12 illustrates the TAPCHAN, the Wave Dragon, and SSG devices.

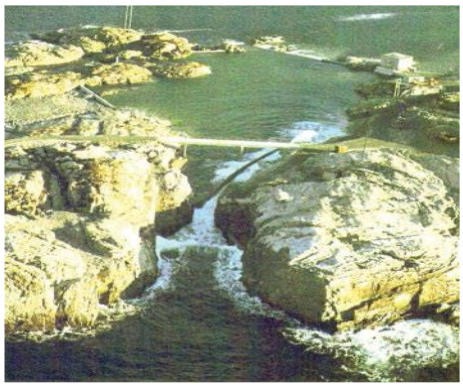

(a)

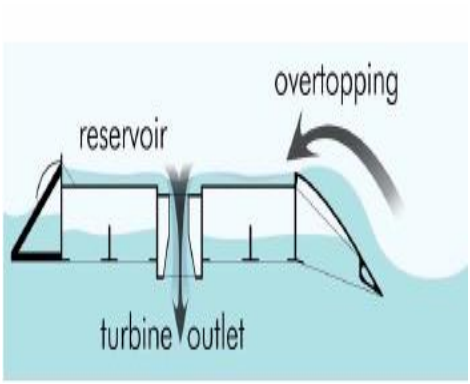

(b

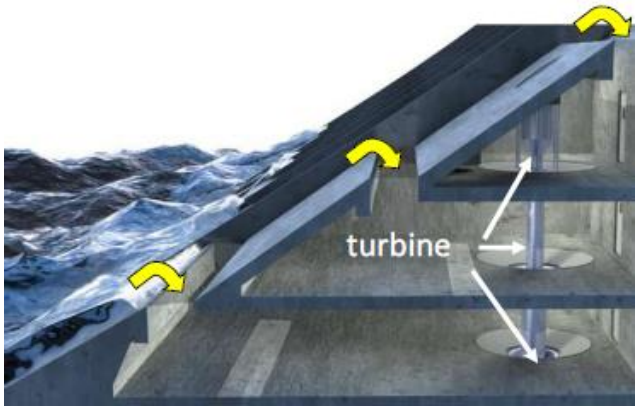

(c)

Figure 12. (a) TAPCHAN (Tapered Channel Wave Power Device) in Norway (Greaves & Iglesias, 2018) (b) the Wave Dragon (Drew et al., 2009) (c) the Seawave Slot-Cone Generator (SSG) (Falcão, 2014).

2.6.3. Classification according to directional dependence

WECs can be classified into terminator, attenuator and point absorber, according to capture of wave direction of devices (Bull & Ochs, 2013). The schematic can be seen in Figure 13**.**

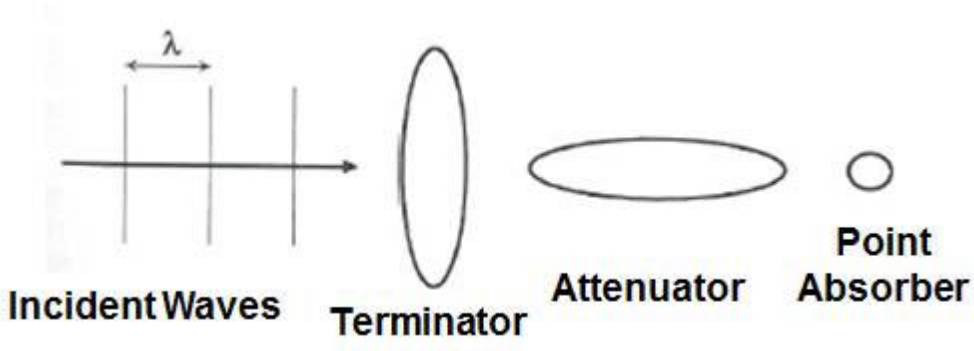

Figure 13. Schematic of directional dependencies (Bull & Ochs, 2013).

Terminator

Terminator devices are able to capture wave energy with devices that are orientated perpendicular relative to the direction of incident wave. The Salter's duck and the Limpet are representative examples of terminator devices (Bull & Ochs, 2013; Drew et al., 2009).

Attenuator

Attenuator devices are comprised of multiple floating segments, which are orientated parallel relative to the direction of incoming wave. The flexing motion of devices derives from the different wave heights, occurring in the segment connected, and this motion drives hydraulic pumps or other converters to produce electricity (Bull & Ochs, 2013; Poullikkas, 2014). The floating attenuators have achieved excellent performance in development, with several examples including the Pelamis and McMave wave pump (Poullikkas, 2014).

Point absorber

Point absorber is able to capture wave energy from all directions, possessing a small horizontal dimension relative to the incident wavelength (Poullikkas, 2014). It is a device that shows a heave movement of one component (a buoy) which is relative to a second component, the bottom end as a fixed component on the seabed. The rising and falling of waves lead to this relative heaving motion that can drive simultaneously generators or other hydraulic energy converters (Bull & Ochs,

2013). Examples of point absorbers are Archimedes Wave Swing, and Seabased buoy device (Lysekil).

2.7. Representative WEC project cases

2.7.1. Classification according to directional dependence

WECs have been developing continuously since the early 1970s. It has taken a long time to develop and commercialize the devices and there are many that have failed to move from small laboratory scale to full or deployment scale.

One of the typical previous project cases is the Salter duck, which was developed by Stephen Salter in 1975 (Yin & Technology Press, 2013). It has a completed design, but for many reasons, this project has never been deployed at full scale on the sea (Robyns, Davigny, François, Henneton, & Sprooten, 2012). Basic details about the development of that with scale are show in Table 3 (Constans, 2013).

Table 3. Testing program of Salter duck project.

Testing program of Salter duck			
Object	**Scale**	**Time**	**Location**
Salter duck project with 24 ducks, 0.5 m long joined with a rigid steel backbone	1:50	1976	Draycote Reservoir, Rugby
Structural backbone initially, then with ducks (2 m long) added; also tests with hydraulics and electrics	1:10	1977	Loch Ness
Backbone and ducks	1:100	1977	University of Edinburgh test tank
Backbone and ducks	1:4	1978	University of Edinburgh test tank

2.7.2. Some commercialised WECs

The Salter duck project did not come to the full scale, but it was still a pioneer WEC project. At present there are a series of commercialized installed full scale or large scale WEC. These are summarised in Table 4.

Table 4. Commercialized WECs (Poullikkas, 2014; Rusu & Onea, 2018).

Type	Device	Capacity (kW)	Installed country
Terminator	blueWave	2500	Australia
	Limpet	500	UK
	Wave Dragon	5900	Denmark
Attenuator	Sea power	3587	Ireland
	Wave star	2709	Denmark, 1:2 scale
	Pelamis	750	Portugal
Point absorber	CETO	400	Australia
	Lysekil	100	Sweden
	Archimedes Wave Swing	2000	Portugal

2.8. Representative WEC project cases

2.8.1. Classification according to directional dependence

Point absorbers is one of representative WECs which are constituted with a floating heave buoy to absorb wave energy by the energy by a Power Take-off (PTO).

The history of point absorbers can be dated back to the late ninetieth century. Leavitt published an earliest patent of point absorbers in 1885 which was a design to compress air by a heaving buoy with racks and gears to pump the water driven by the wave force. The theory of heaving buoys was developed in the 1900s combined with the research into the hydrodynamics of ships and marine structure (Al Shami, Zhang, & Wang, 2019).

In terms of the experimental development, some scaled point absorbers were tested in Japan in the 1980s and later in Norway, and wave tank and sea tests with large scaled devices have also been conducted (Al Shami, Zhang, et al., 2019).

Point absorbers can be categorized into two types which are one-body point absorber and two-body point absorber. As the name applies, one-body point absorber has only one floating buoy, while a submerged buoy is between the floating buoy and structure body on the seabed for the two-point absorber design (Al Shami, Zhang, et al., 2019).

2.8.2. One-body point absorber

One-body buoy point absorber are the simplest type of all WECs which is mainly combined with a cylindrical, spherical or a hollow cylinder floating buoy connecting to a fixed body on the seabed by a rope. A PTO is set between the floating buoy and the fixed body to convert and harvest electricity through the kinetic energy of the oscillation of floating buoy (Al Shami, Zhang, et al., 2019). A schematic of point absorber is shown in Figure 14.

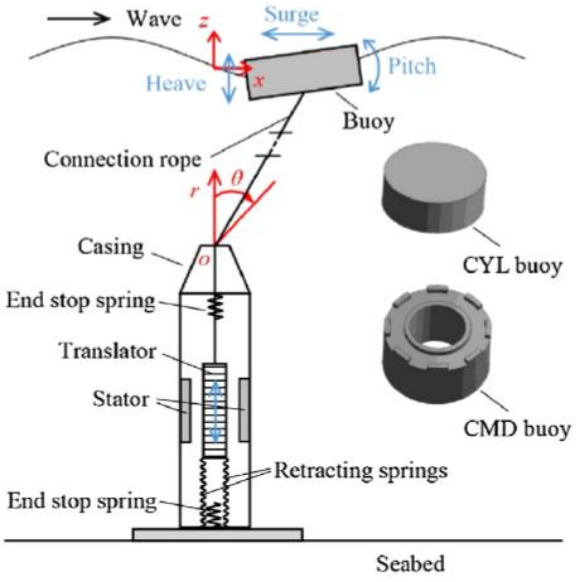

Figure 14. The schematic of a point absorber (Al Shami, Wang, Zhang, & Zuo, 2019)

The study of one-body point absorber focuses on dynamics and hydrodynamics. The dynamics of this type of WEC is investigated in the time domain or frequency domain. The time domain highly depends on computation, and mainly analyse nonlinear elements including nonlinear wave excitation forces, complex mooring

and so on. These nonlinear elements analysis can be simulated by a non-linear numerical model or a computational fluids dynamics (CFD) based on finite element analysis simulation (FEA) with a point absorber placed in a numerical wave tank. On the other hand, although frequency domain cannot study nonlinear elements, it is a simple study without computation requirement (Al Shami, Zhang, et al., 2019).

The hydrodynamics of point absorbers is a branch of ship motions to figure out the problems in two parts which are effect of wave pressure on a fixed-point absorber, and radiated waves from oscillation of point absorber under the still water condition (Al Shami, Zhang, et al., 2019).

The theory of one-body point absorber has been developed mainly in design, optimizations, and parametric studies. For example, a study about the resonance of a point absorber under regular and irregular sea conditions was conducted by Yavuz, McCabe, Aggidis and Widden (Yavuz, McCabe, Aggidis, & Widden, 2006). In their study, they developed a prediction algorithm to predict the frequency of incident waves and main short frequency of irregular waves in order to optimize the performance of device by adjusting PTO parameters.

Pastor and Liu (Pastor & Liu, 2014) studied a numerical simulation of point absorber in time domain, frequency domain, different shapes, parameters and drafts. The optimum results from this simulation indicated that the capture power was not affected by shapes. It concluded that the generating capacity was overestimated by traditional linear boundary element methods was derived from the study of Giorgi and Ringwood. They compared the output power with the traditional linear estimation method from a non-linear CFD simulation of latching control to a heaving point absorber.

The development of experiment one-body point absorbers also goes hand in hand. Wave tank experiments can be used to validate the mathematical models and simulation in order to optimize the design further. Moreover, wave tank

experiment is convenient to investigate some cases, especially complex wave theories and non-linearity (Al Shami, Zhang, et al., 2019). For example, Göteman, et al. (Göteman et al., 2015) conducted a wave tank experiment to investigate response of a heaving buoy under the extreme waves condition using a 1:20 scale device. In this test, three buoys connected to a linear PTO respectively were used and simulated by a friction damping mechanism under regular and irregular conditions. The results presented a various measured wave forces at the same wave height which indicated the relationship between PTO damping and absorbed wave forces.

2.8.3. One-body point absorber

The structure of a two-body point absorber is added a submerged body which can be oscillated under the floating buoy with the PTO placed between the two bodies. By this design, the total mass of the device is increased due to the submerged body with the increase of added hydrodynamic mass, so the natural frequency of the system will be reduced. This causes a high efficiency of capture power because of inducing relative motion easily between the oscillating buoy and the submerged buoy (Al Shami, Zhang, et al., 2019). Two designs can be seen in Figure 15, and a capture efficiency comparison of one-body and two-body point absorber is in Figure 16.

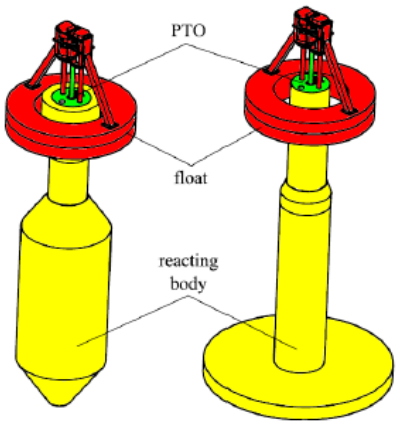

Figure 15. Wavebob and Powrbuoy (Al Shami, Wang, et al., 2019).

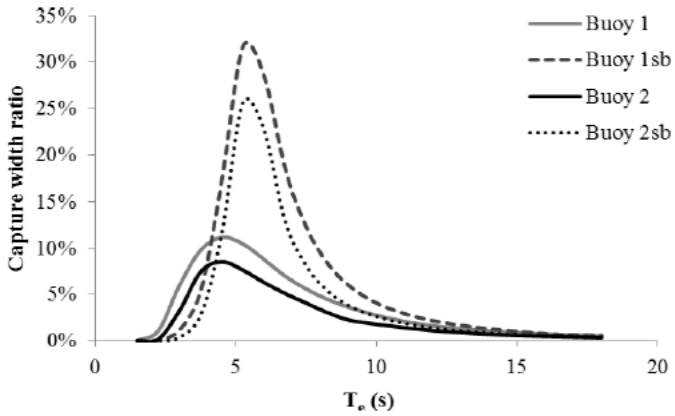

Figure 16. Power capture width ratio comparison (Al Shami, Wang, et al., 2019).

The analysis of two-point absorber dynamics was first performed by Falnes (Al Shami, Zhang, et al., 2019). It was an analysis about dynamics equations of a two-body point absorber working in the frequency domain with a linearized viscous damping force, and got the maximum theoretical absorbed power under the different assumptions and oscillating modes.

Liang and Zuo (Liang & Zuo, 2017) did an analysis of a two-body point absorber in the frequency domain with a linearized viscous damping form. The result presented that the efficiency of captured power was decreased due to the viscous damping. Thus, the two-body system should be modelled accurately in the time domain.

The hydrodynamics of two-body point absorber is similar with that of one-body point absorber. Falnes was also the first to come up with the possibility of elimination of the interaction of hydrodynamic coefficients by the dynamics equations which is less than the one-body specific hydrodynamic coefficients. The boundary element method was mostly used to establish the simulation of the hydrodynamics coefficients of a two-body point absorber system by some high efficient and accurate software such as ANSYS Aqwa and WAMIT focusing on the individual hydrodynamic properties of submerged body and the interactions between the two oscillating bodies (Al Shami, Zhang, et al., 2019).

The two-body design has been proven theoretically to capture more power than that of one-body design under the low resonant frequency which is closed to the real frequency of sea waves. The theoretical development of two-body point absorber has not been ended up in design, optimizations and parameter researches (Al Shami, Zhang, et al., 2019).

For example, a CFD simulation of a two-body heaving point absorber based on the Reynolds-Averaged Navier-Stokes equations was conducted by Yu and Li (Yu, Li, & Fluids, 2013), which focused on the heave response to the absorbed power. The results presented the nonlinear wave interactions and viscous effects. Amiri, et al. (Amiri, Panahi, & Radfar, 2016) established a linear mathematical model of a two-body point absorber in the time domain and frequency domain with the hydrodynamics calculation by ANSYS Aqwa. Under the conditions of different sea states, PTO damping coefficient and the buoy shapes, the results indicated that a cylindrical and a conical bottom buoy with a small draft can absorb the most power. In terms of the optimization, Al Shami, et al. (Al Shami, Wang, et al., 2019) did a research in parameter using Taguchi method, and according to the results, the captured power and bandwidth were increased with the reduction on the resonance frequency which means the shape of submerged body was likely to influence the capture and the resonant frequency.

In terms of the development of experiment, wave tank experiments are also used to simulate and validation the two-body point absorber devices. However, the wave tanks are subject to shallow depth so that it is not suitable to place a device with a submerged body at a specific depth from the water surface. Moreover, the added submerged body increases the complexity and freedom degrees of the whole device system (Al Shami, Zhang, et al., 2019).

Nevertheless, the wave tank experiments of two of the most representative two-body point absorbers which are the WAVEBOB and POWERBUOY have been conducted by Beatty, et al (Beatty, Hall, Buckham, Wild, & Bocking, 2015). The tests

only focused on the heave with 1:25 scaled models. The results validated that the numerical results were matched with the experimental results. The conclusion indicated that each device is adequate for a specific sea condition because of the different shape of submerged body. The streamlined submerged body of the WAVEBOB led to decrease of the viscous drag force so that the device can capture more power, and the POWERBUOY presented a low natural resonant frequency on account of the heavy mass of the submerged body.

2.8.4. Power take-off (PTO)

The PTO is the important part of power capturing, and transfer the absorbed mechanical energy to electricity. The PTO use mainly two types of generators which are linear generators and linear to rotary generators (Al Shami, Wang, et al., 2019).

The linear generators are driven by a spring and a permanent magnet and have a better working performance under the low velocity and high force conditions, especially suitable for heaving point absorbers. This type of generator is related to the heave dynamics of the WEC without a mechanical interface to transmit the motion mode, so it leads to increase the capture efficiency with less maintenance.

In Figure 17, a snapper PTO with a large spring drives a direct-drive linear generator by high forces. BY this way, when the spring force is higher than the magnetic force, the relative velocities of motion will be increased in a short time so as to enhance the product of power during the same time.

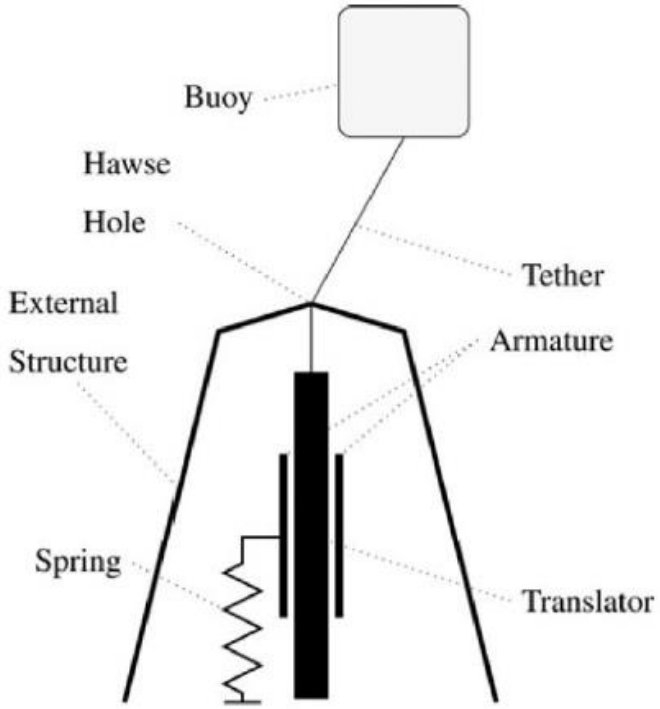

Figure 17. Schematic of a snapper PTO (Al Shami, Wang, et al., 2019).

Compared with the expensive permanent magnet linear generator, an alternative design has been proposed. The system equips a cheap dc or ac synchronous generator. The mechanism of this design is to transfer the translated heave motion into a rotary motion under a mechanical system. Although the added mechanical parts cause additional maintenance, this simple design with low cost is feasible to be commercialized. A crank slider design is similar to a conventional combustion engine, shown in Figure 18. Figure 19 presents a novel PTO, ant the mechanism is that a contactless force transmission system based on permanent magnets transmits the wave forces to the PTO. The force will drive a ball screw to transfer the linear motion into rotary one (Al Shami, Wang, et al., 2019). Table 5 summarizes a variety of novel PTOs.

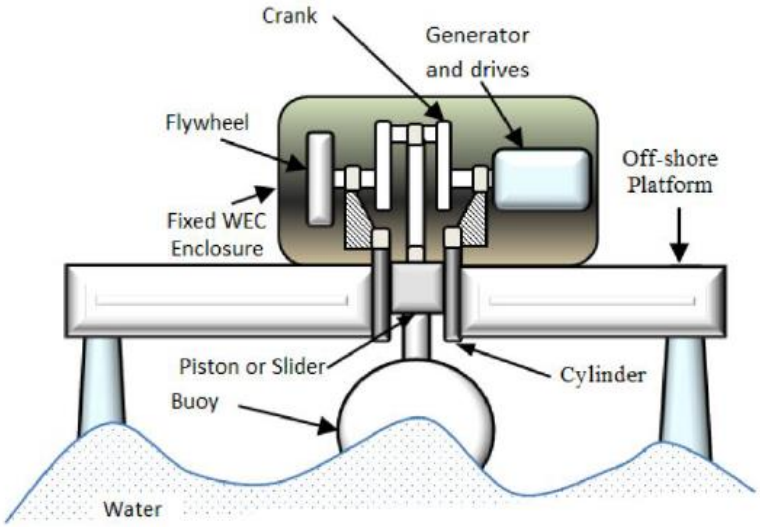

Figure 18. Schematic of a crank slider (Al Shami, Wang, et al., 2019).

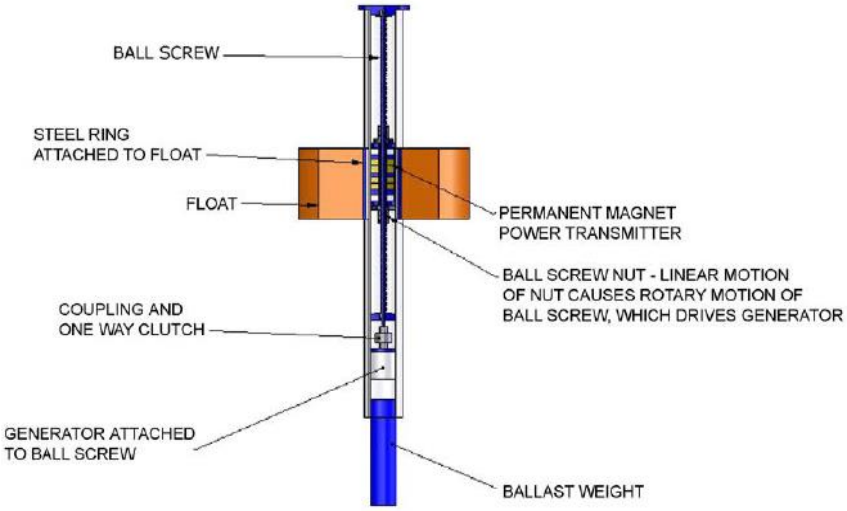

Figure 19. Ball screw mechanism (Al Shami, Wang, et al., 2019).

Table 5. A summary of novel PTOs.

Design	Type	Tested/Scale	Highest efficiency	Target
Transverse-flux permanent magnet	Linear	Yes/Full scale	>90%	AWS
Snapper spring system	Linear	Yes/Full scale	N.A.	Full scale point absorbers
Crank slider mechanism	Linear to rotary	No	N.A.	Full scale point absorbers
Ball screw mechanism	Linear to rotary	Yes/ scaled to wave tank experiments	60%	Full scale point absorbers

2.9. Wave resource assessment

2.9.1. Classification according to directional dependence

Wave energy derived from the wind energy as the wind blowing over the ocean with the energy transfer. In this wave field, a collection of sea wave travel from different directions with various frequencies, which is characterized by a directional wave spectrum (Board, Council, Marine, & Committee, 2013).

The wave resource assessment is to measure the quantity of power flux from sea area. In order to estimate the theoretical resource, wave power density as the energy level is usually introduced and expressed as power per unit length of wave crest, which means the all energy travel a vertical plane of unit width during a unit time, and this vertical plane extends from the sea surface to the seabed, oriented

by the wave crest (Board et al., 2013). A typical high value range of wave power density is from 20 to 70 kW/m in offshore locations, existing at mid and high latitudes (NikWB, Sulaiman, Rosliza, Prawoto, & Muzathik, 2011).

The wave energy assessment is a prerequisite for design and deployment of WECs with estimation of wave climate from uncertainties including variations of seasons and years. Thus, the purpose of resource assessment is to provide a prediction of available energy production and traits of operating and survival in a specific site, and to identify the seasonal and annual variations for the production of potential energy (Ingram, 2011).

The wave resource assessment provides a quantified estimated of the available energy resource, and also assesses the operating and survival characteristics of a specific site around a coastal region. This assessment is presented by data in different ways which are H_{m0}-T_e scatter plots, parameter time series, 1D spectral plots and 2D polar spectral plots, where H_{m0} and T_e represent significant wave height and energy wave period respectively (Ingram, 2011).

For each method, it requires data of different timescale and purpose of assessment. The requirement of data can be categorized into three parts by time.

Long-term assessments require a minimum ten years of data to present yearly and seasonal variations of resource level. The scatter plots with parameter of H_{m0} and T_e give the summary of those variations (Ingram, 2011).

For medium-term assessment, the data should be more than one year to predictions. The scatter diagrams are required to be presented by monthly or yearly plots, and the spectral data should be in 1D or 2D polar plots.

Short-term cases are presented in short timescale by days or hours during a relatively short time. The 1D or 2D polar plots are also suitable to be used for presentation of short-term cases (Ingram, 2011).

A H_{m0} against T^* plot should be established in scatter diagrams. T^* could be T_0, the

mean wave period, T_p, the peak wave period and the energy wave period, T_e.

The average wave power should be calculated by H_{m0}-T_e plots in scatter diagrams, and scatter diagrams provide the summary of the yearly wave resource. Additionally, seasonal diagrams are also be presented in spring (March, April May), summer (June, July, August), autumn (September, October, November), and winter (December, January, February) (Ingram, 2011).

There are some requirements (Ingram, 2011) of scatter diagrams following below:

- For each bin, it should present the cumulative occurrences of the H_{m0} -T^* pair, and normalised scatter diagrams could be given with the total number of the data points.
- H_{m0} bins are to be defined in 0.5 m intervals over the range from 0.5 m to 15 m.
- Wave period bins are to be defined in 0.5 second intervals over the range from 0.5 seconds to 25 seconds.
- The boundaries of bins have a relationship: *limit* < H_{m0}, T_e ≤ upper limit.
- The minimum and maximum bins have no lower and upper limitations respectively.

This assessment as a mathematical demonstration provides the distribution of wave power in various spaces and time from wave data. The mean power level can be expressed as Equation 1 (Ingram, 2011):

$$J = \frac{\rho g^2}{64\pi} T_e H_{m0}^2 \quad (1)$$

where J is the energy flux per unit of wave-crest length, g is the gravity acceleration, ρ is the sea water density, H_{m0} is the significant wave height and T_e is the energy wave period.

3. Methodology

Chapter 3 contains the physical description of the wave energy device that was designed and manufactured and the corresponding mathematical model. This chapter also describes the experimental procedure undertaken to investigate the free and forced response of the two proposed iterations of the device as well as determining the corresponding Response Amplitude Operators (RAOs).

3.1. Selection of device

The design of the device proposed in this project was based on the WEC currently being developed by Seabased (*The Technology*). The Seabased WEC has been well-developed, and the viability of the technology has been demonstrated through a number of projects, the most recent being a demonstration wave energy park along the coast of Ghana (Harris, 2018), which is depicted in Figure 20. This technology has a series of advantages over other WECs that are currently in development; namely, it has been optimised for nearshore locations, has a modular design, can be easily integrated into grid, and has proven survivability in the harsh marine environment.

Figure 20. Seabased Ada Foab Pilot Wave Energy Farm in Ghana (Seabased, 2020).

3.2. Experiment set up

3.2.1. WEC design

According to the five-stage developmental programme (Figure 21) utilised by the wave energy sector, the first stage of developing a WEC is to determine the performance of the proposed device, which coincides with Technology Readiness Levels (TRLs) 1-3. WECs at this stage are considered small-scale (1:25-100).

An approximate 1:50 scaled model of the selected WEC was constructed in the University of Waikato engineering workshop. As seen in the engineering drawing (Figure 22) and the detailed schematic (Figure 23), the proposed device is comprised of a clear tube that is covered on either end. The PTO mechanism, a linear generator, is modelled using a spring, which is connected with a small hook to the bottom cover and to a rod that runs through the top cover. An O-ring is housed in the top cover, and this component plays an essential role as it ensures that the tube is and remains watertight. A wire then connects the outer end of the

rod to a buoy, and the whole model is fixed to a foundation. There are two iterations of the device, as two different springs with varying stiffness are used in the testing programme.

The final constructed device is shown in Figure 24 and its main components are reported in Table 6.

Figure 21. International structured development plan (Holmes & Nielsen, 2010).

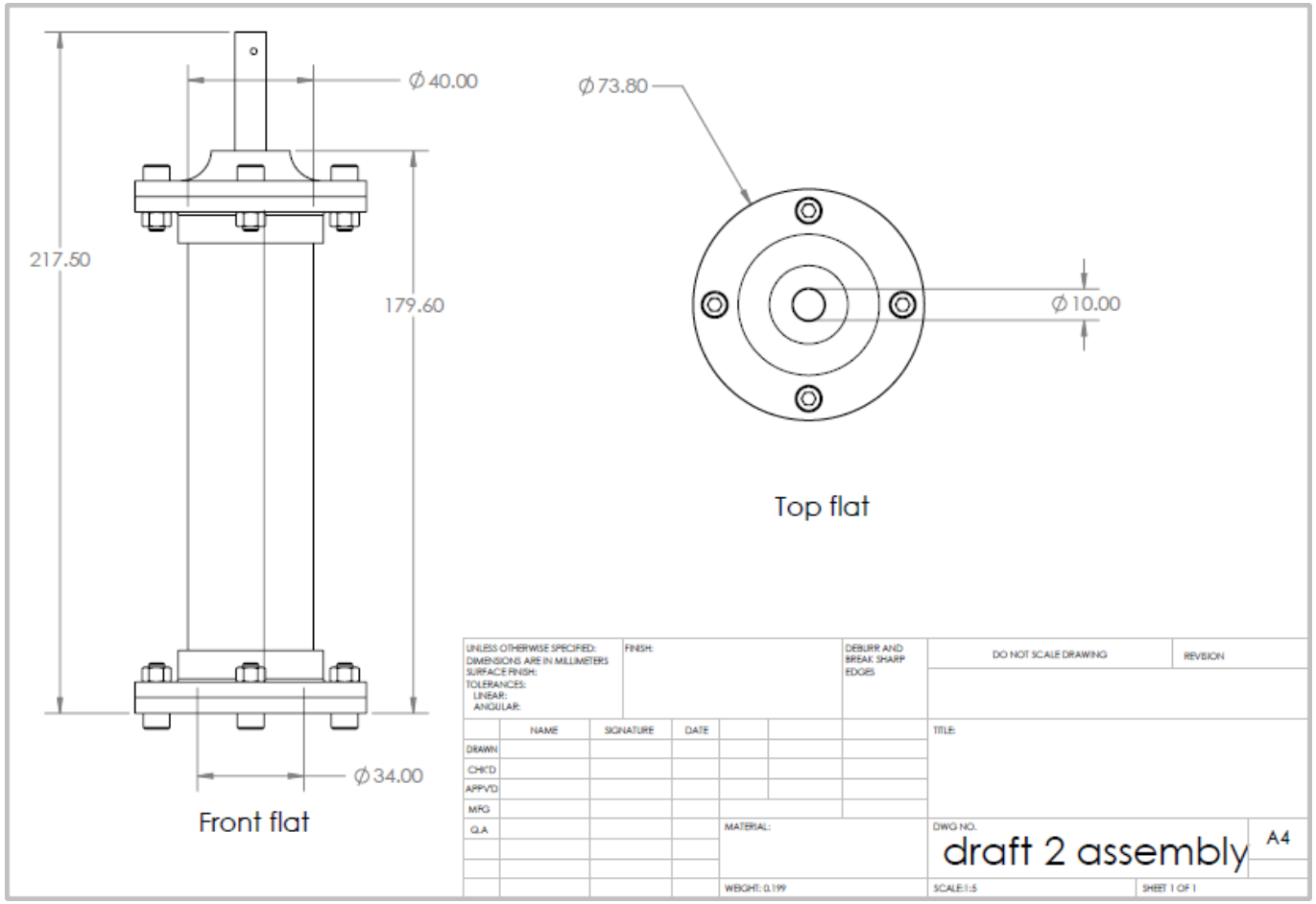

Figure 22. Engineering drawing of the proposed WEC.

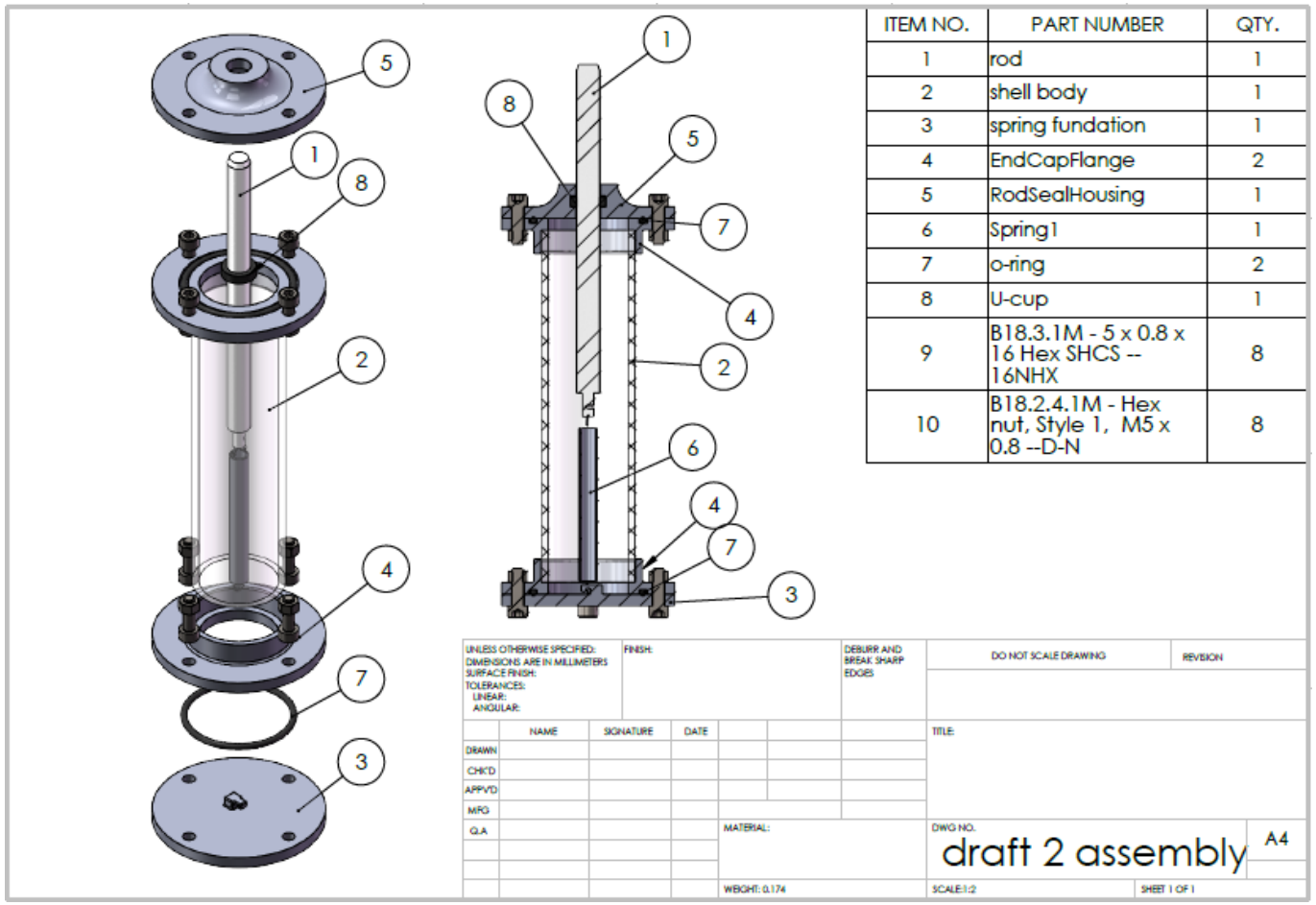

Figure 23. Schematic representation of the assembly of the proposed physical model.

Figure 24. The final constructed experimental scale model of the wave energy converter.

The sealing component, the O-ring, is a product of Seal Imports Ltd (UM01001504) with the following dimensions: 4 mm height, 10 mm inner diameter and 15 mm outer diameter.

The spring constant of each spring was measured using a force scale and applying Hooke's law:

$$F_k = -kx \tag{2}$$

where F_k is the restoring force, k is the spring constant and x is the amount that the spring extends (in m).

Table 6. Key components of the final constructed 1:50 scale WEC.

Component	Measurement
Height of model body	217 mm
Diameter of covers	73.8 mm
Diameter of tube	40 mm
Diameter of rod	10 mm
Height of buoy	80 mm
Diameter of buoy	100 mm
Weight of buoy	122 g
Length of wire	10 mm
Length of Spring 1	35 mm
Constant of Spring 1	192 N/m
Length of Spring 2	35 mm
Constant of Spring 2	72 N/m

3.2.2. Apparatus and facility assembly

Typical laboratory testing of a WEC requires several key experimental apparatus, such as an appropriately sized wave flume, wave-maker(s), and measurement systems that capture and record the raw data pertaining to the device's motion, velocity, and force (Payne, Taylor, & Ingram, 2009). However, the available equipment to conduct the relevant tests for this project was severely limited, and therefore a simpler method was proposed and applied, which is discussed below.

Water tank and trolley

As there was no appropriately sized wave flume with a wave maker in the facilities provided, it was decided that the waves would be generated manually by utilising

a water tank and trolley. The water tank (Figure 25) is 550 mm in height and 390 mm x 390 mm in length and width and was placed on top of the trolley (Figure 26) with dimensions of 900 mm x 600 mm.

In order to generate the waves, the investigator pushed the trolley back and forth, which changed the original still water to a fluctuating state. This movement of water produced a wave because of the inertia from the motion of trolley and water tank in its entirety. Thus, successive wave-making could be achieved in this manner.

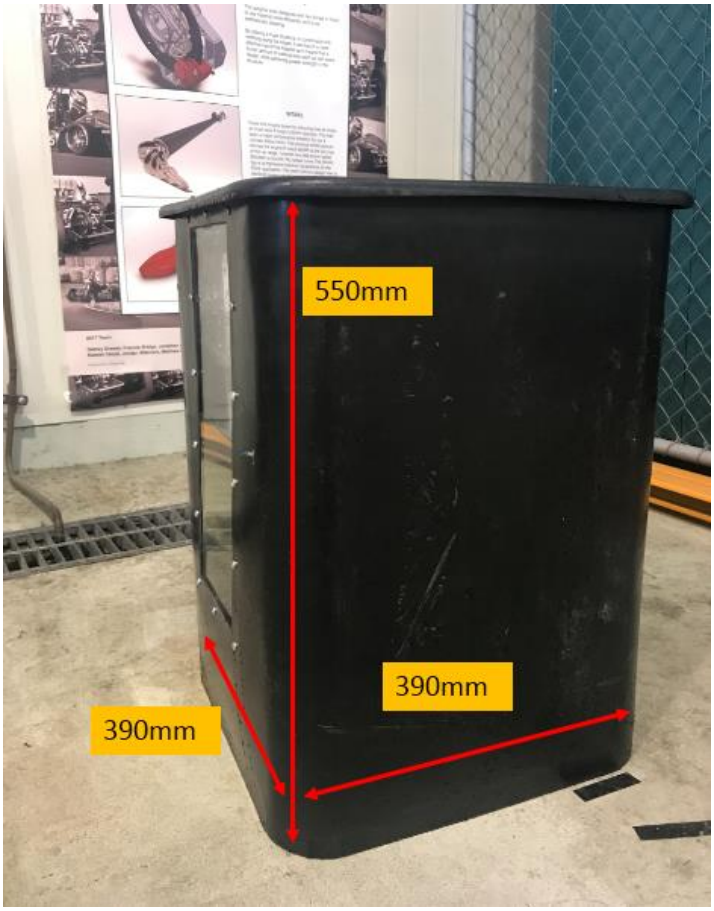

Figure 25. The testing tank.

Figure 26. The trolley utilised to generate the waves.

In order to monitor and record the motion of the buoy and the generated waves, the water tank was modified with the addition of 'windows'. The front and the sidewall of the water tank were removed and replaced with transparent sheets of plastic. The front-facing window had dimensions of 360 mm x 460 mm, while the side-facing window had dimensions of 460 mm x 255 mm. The modified water tank is depicted in Figure 27.

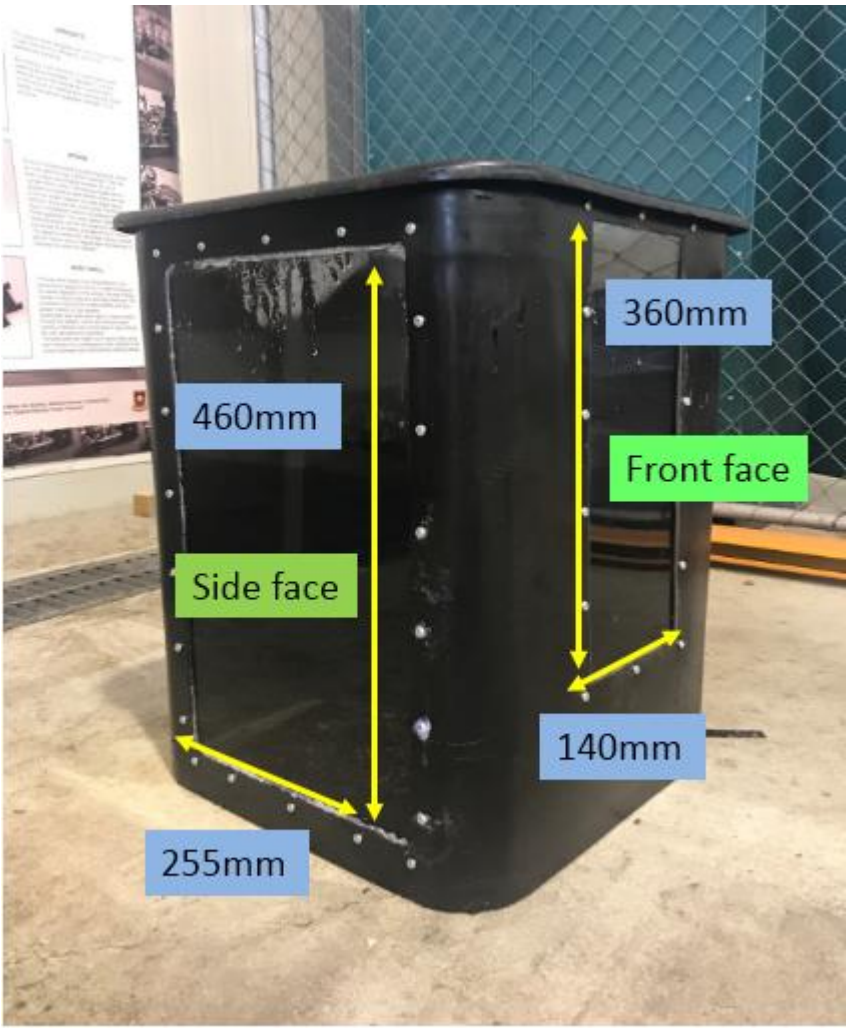

Figure 27. Picture of the testing tank with viewing windows.

Measurement of wave and buoy motion

The magnitude of the buoy motion was measured by using a ruler and reference point (a portion of black tape on the shaft of the device). The movement of the buoy was assumed to be the same as the change in spring length.

Figure 28 depicts the proposed arrangement, with the ruler attached rigidly to the black base place (which modelled the WEC foundation).

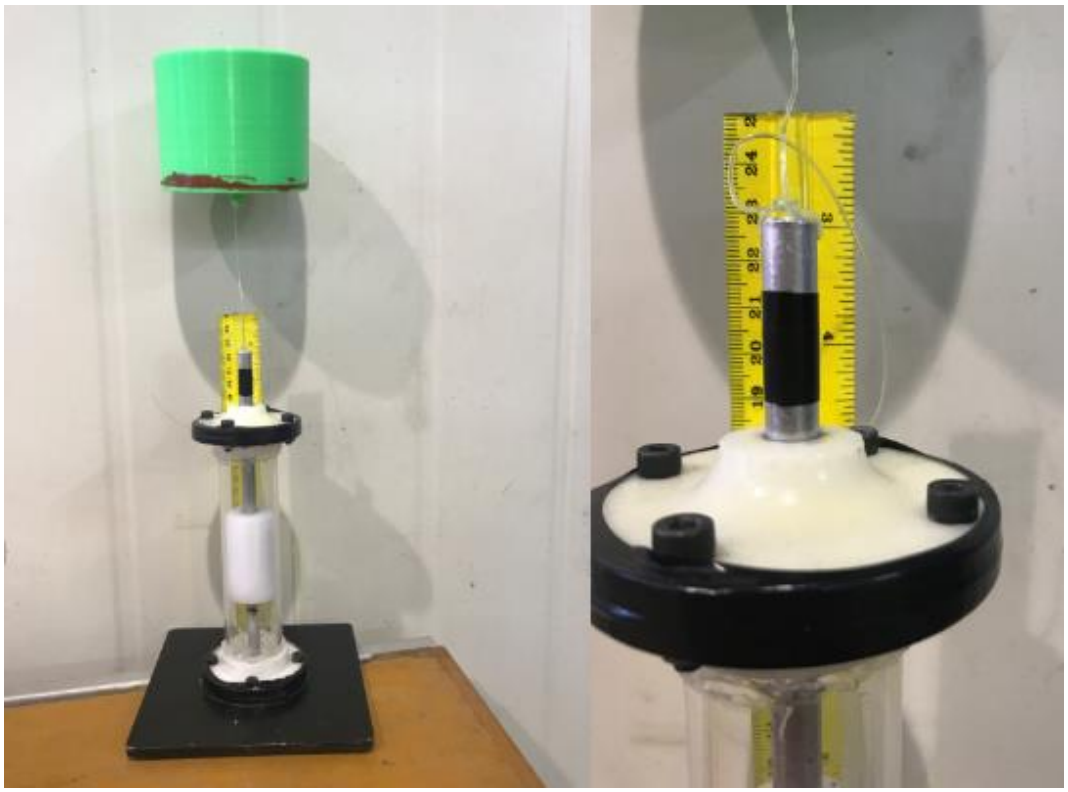

Figure 28. Experimental WEC model.

As seen in Figure 29, two rulers were mounted on the side-facing window of the water tank to measure the displacement of the generated wave. Ruler 1 was transparent and was placed horizontally at approximately the still water level, while Ruler 2 was fixed flush along the length of the water tank window.

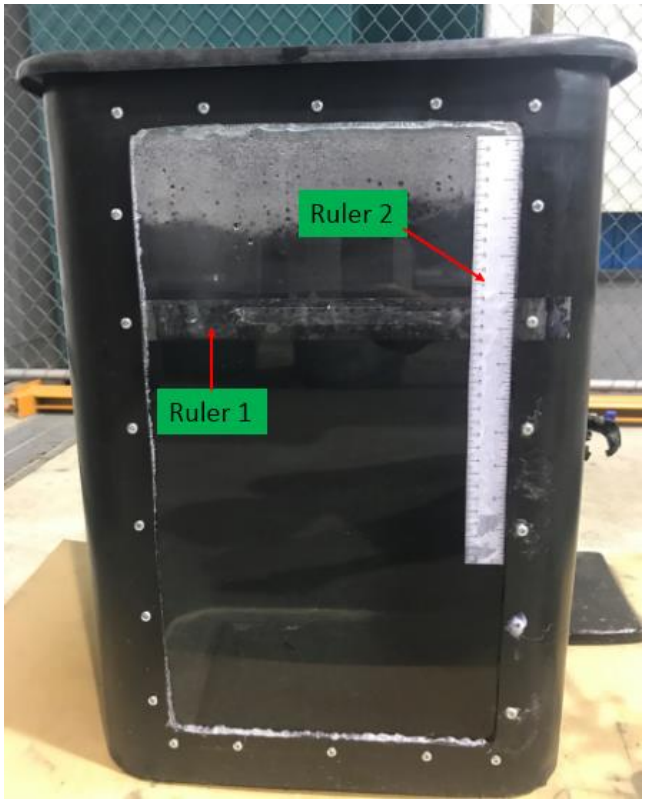

Figure 29. Rulers used for measuring the generated wave.

Retort stands and Camera

During the experiments, the motion of the buoy and the corresponding generated waves were recorded. An iPad was used to record the behaviour of the wave buoy (front-facing window), while a smartphone was used to capture the behaviour of the generated wave (side-facing window). Both devices were fixed to the trolley via retort stands. The entire experimental configuration is illustrated in Figure 30, which was comprised of a water tank, trolley, cameras (iPad and smartphone), and the physical model of the proposed device.

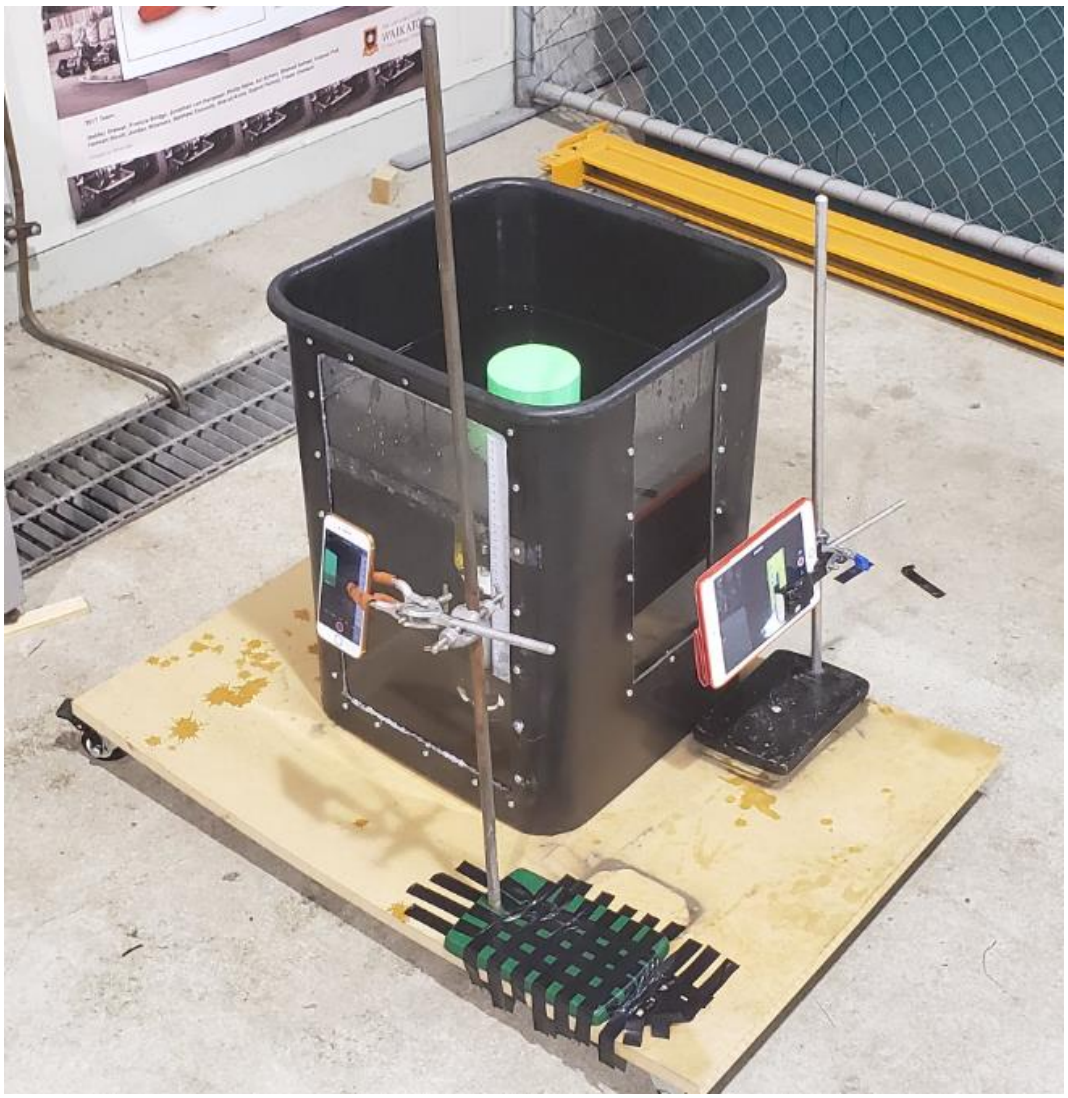

Figure 30. Entire experimental set-up.

3.3. Experimental procedure

Two separate sets of experiments were conducted. The first was to measure the free response of the system under still water conditions. The second was to measure the forced response of the system. Both sets of tests were conducted for two iterations of the proposed device. The first iteration utilised a soft spring (Spring 2), whilst the second iteration used a stiffer spring (Spring 1). The test and test procedures are outlined and discussed below.

3.3.1. Free response of the system (Still water test)

The objective of this test is to determine the natural frequency of the device in heave.

Procedure

1. Fix the device's baseplate to the bottom of the water tank and allow it to settle.
2. Push the buoy down vertically just under the water level and then release it.
3. Record the oscillations of the buoy (from the first extreme) with a camera and time the duration of the test run.
4. Repeat steps 1 – 3 several times.
5. The natural period is determined by averaging the results from the test runs, which is calculated by dividing the duration of each test by the number of device oscillations.

3.3.2. Forced response of the system

The forced response of the system water tests is comprised of irregular and regular wave tests. For the irregular wave test, the aim is to investigate the performance of the physical model in panchromatic wave conditions. In contrast, the regular wave test will examine the performance of the buoy under monochromatic wave conditions. The fluctuations of the buoy, in both tests, are illustrated by the change in the length of the spring being analysed.

Procedure

1. Place the model device in the centre of the water tank, and the fix the device's baseplate to the bottom of the tank.
2. Measure the buoy's draught line, and ensure that the wire connecting the buoy to the rod is taut.

3. Push and pull the trolley repeatedly to generate waves and record the oscillations of the device using the cameras.

    a) For irregular waves, the investigator pushes and pulls the trolley at random intervals. (These tests are between 8 to 12 seconds in duration.)

    b) For regular waves, the trolley is pushed from mark 1 to 2 and pulled back from mark 2 to 1 for two seconds at regular intervals (Figure 31). The duration time of the test requires at least 15 seconds to ensure getting enough data.

4. Stop the recording and wait for the still water state to be achieved.

5. Repeat the Steps 2 to 4 two more times for the regular wave tests.

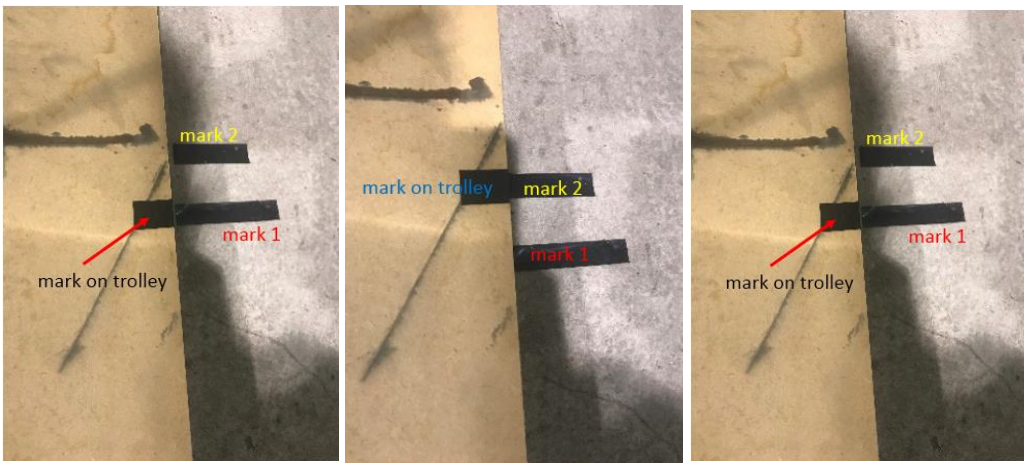

Figure 31. Picture of the movement between mark 1 and mark 2.

3.4. Data analysis

There are two basic ways to analyse and illustrate the test results, namely time and frequency domain (Holmes, 2009). Time domain analysis has been used in this report, which according to Holmes (2009) can determine the following parameters of the WEC model being analysed:

- phase relationship
- amplitude of each parameter

- response of regular excitation
- resonance proximity
- quality of signals
- signal statistics

A number of these parameters can be determined from the tests outlined in Section 3.3. The raw data obtained from these experiments can be plotted in a displacement vs time graph (Figure 3), which shows the performance and characteristics of a specific device configuration. Therefore, the two iterations (soft vs stiff spring) of the device can be compared.

In order to read and get the most useful information from the raw data, every recording is investigated frame by frame using the freely available Movie Maker application. This will require the investigator to first filter the quality of the videos.

For the regular wave tests, both the wave and device displacement is required, while the irregular wave tests only require the device displacement values. Figure 32 and Figure 33 depict the procedure for obtaining the crest (highest water level position) and trough (lowest water level position) measurements of the generated wave.

While Figure 34, Figure 35, and Figure 36 depicts the process for obtaining the device displacement. The top of the black tape (located on the rod) is used as the reference line (Figure 34), and the difference between the highest reading (Figure 35) and reference line is the crest value of the spring (device). The difference between the lowest reading and the reference line is the trough value of the spring (device), which is depicted in Figure 36.

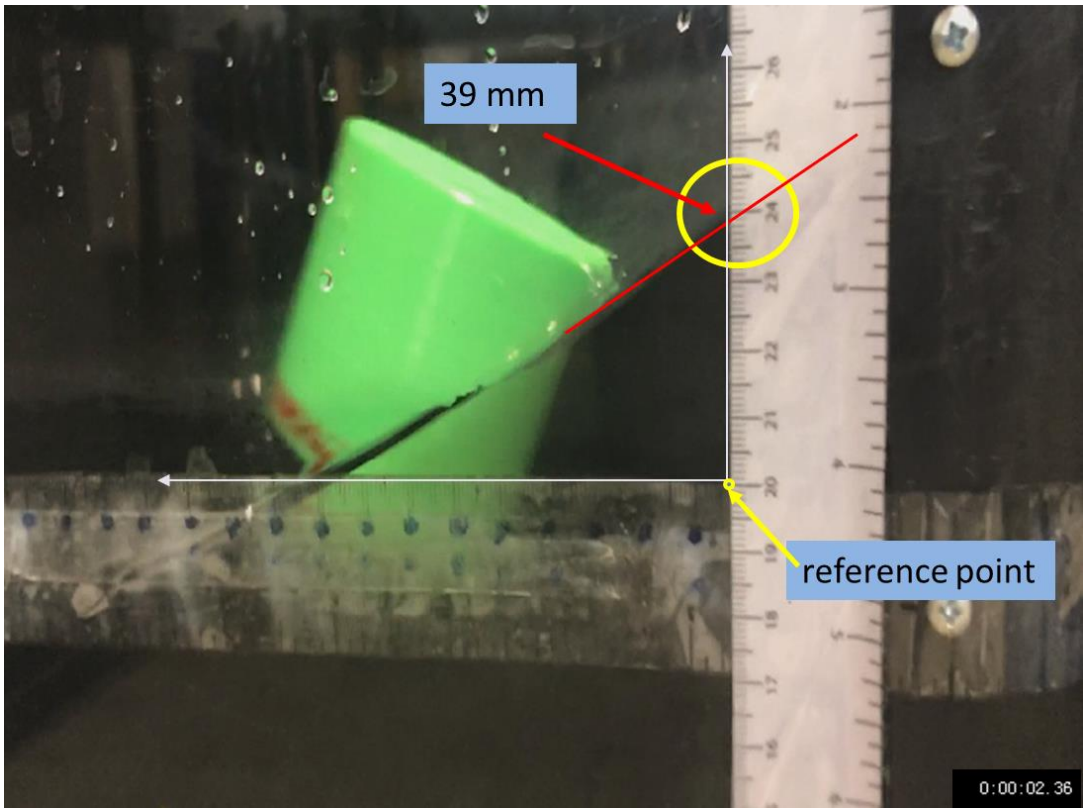

Figure 32. Generated wave crest reading, with corresponding time.

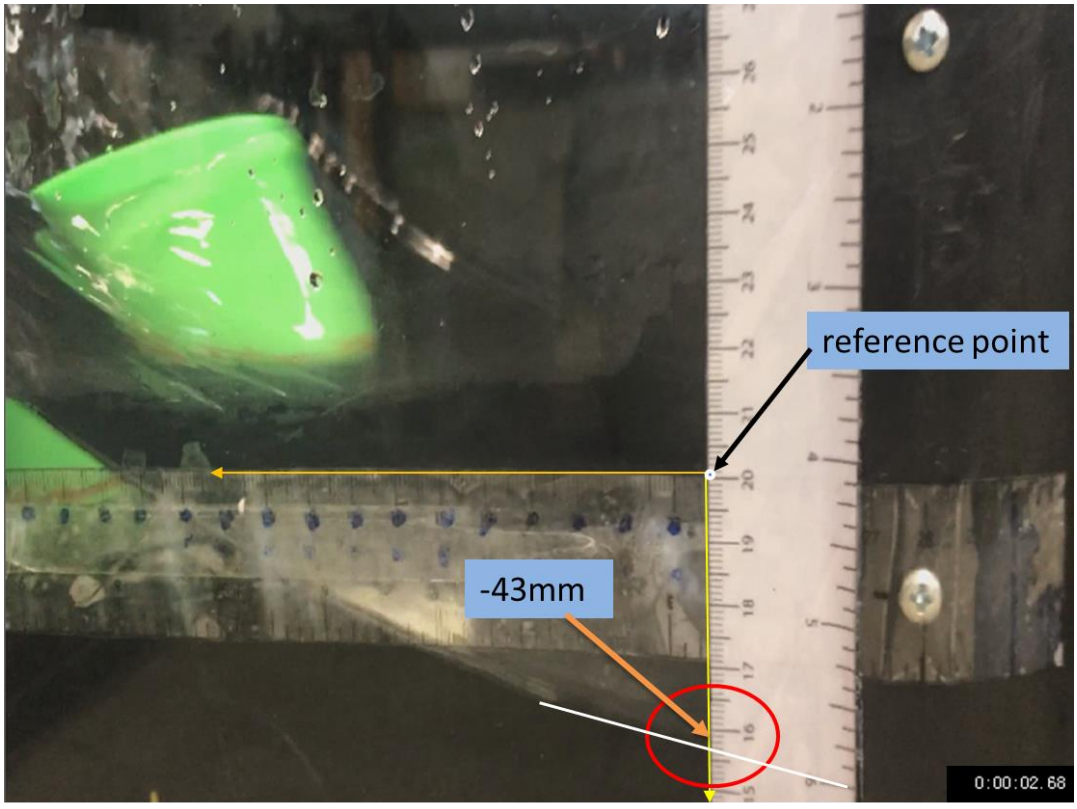

Figure 33. Generated wave trough reading, with corresponding time.

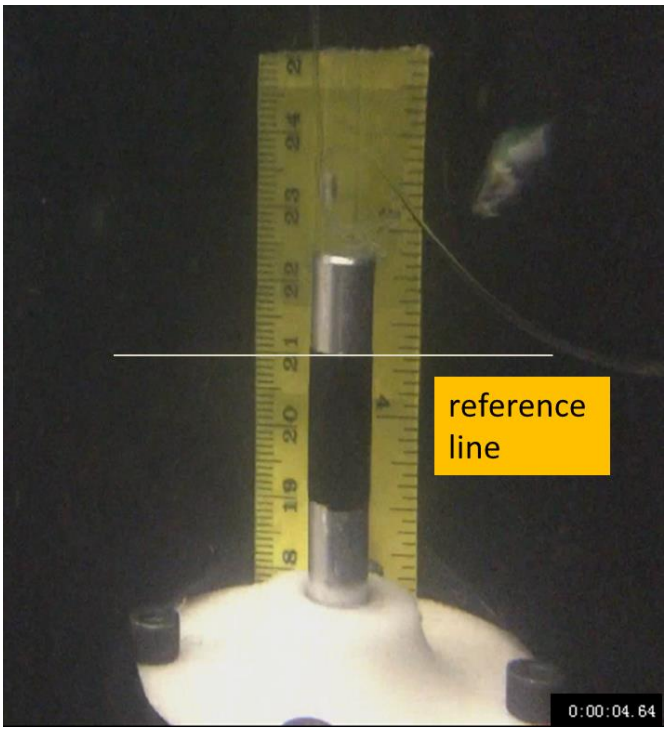

Figure 34. The reference line with the corresponding time.

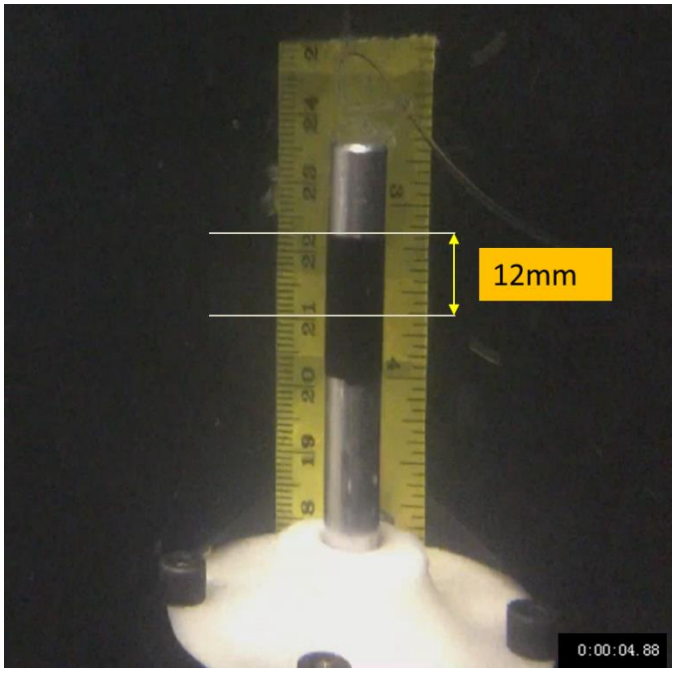

Figure 35. The (highest) reading of an oscillation of spring with the corresponding time.

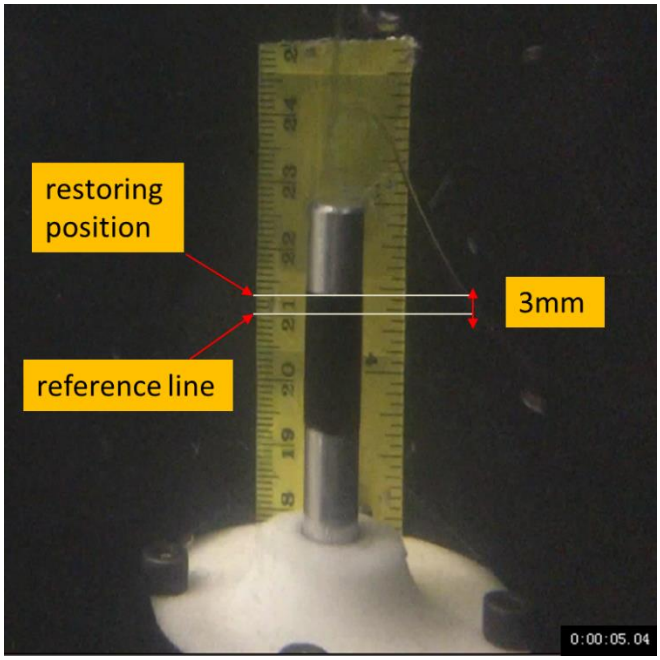

Figure 36. The (lowest) reading of restoring position with the corresponding time.

3.4.1. Response Amplitude Operator (RAO)

Sea waves are an important aspect of the marine environment as it causes floating bodies, such as ships and buoys, to oscillate. The motion of sea waves can be regarded as a kind of irregular movement of water in time and space, and this irregular motion induces irregular movement in a floating body. Thus, it is essential to describe the complicated sea waves' motion. According to the principle of superposition, these complex motions are able to be depicted as the linear superposition responses acting on floating bodies of all wave components with various lengths, amplitudes and propagating directions (Misra, 2015).

If there is a proportional relationship between the response of the floating body to the incoming regular wave, it can be characterised by using RAOs. The RAO is the ratio between the response amplitude (of the floating body) and the amplitude of the regular wave with a specific frequency (Misra, 2015). The RAO is composed of two parts; the Response Amplitude and Operator. The Response Amplitude refers to the degree of the actual or absolute motion on the floating body, which is generated by a passing hydrodynamic wave. The Operator is a factor that a

particular value can amplify the response (of the floating), for example, the amplitude of a wave (Aird, 2018).

The RAO non-dimensional equations are (Greaves & Iglesias, 2018):

$$RAO_i = \frac{|\Xi_i|}{a/l^{\gamma}} \quad (3)$$

where Ξ_i is the amplitude of body displacement corresponding to mode i, a is the amplitude of the wave, l is the width or diameter of the floating body, and the exponent γ is 0 for the translational modes (heave, sway, and surge) and 1 for the rotational (yaw, pitch, and roll) modes. Therefore, RAOs can be used to describe the motion of a passing hydrodynamic wave that acts on the floating body in six degrees of freedom (mode). These degrees of freedom are illustrated in Figure 37 (Aird, 2018; Das & Baghfalaki, 2014)

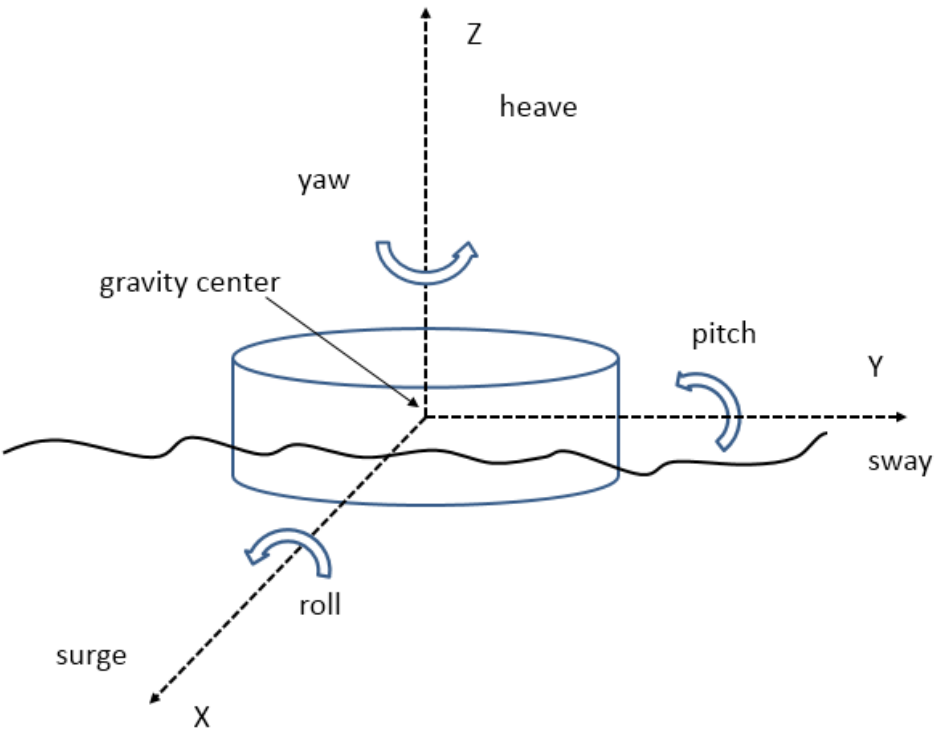

Figure 37. Schematic of degrees of freedom on a floating body.

The proposed device in this experiment is a point absorber constrained to move only in the vertical direction (heave motion). Therefore Equation 3 can be rewritten as:

$$RAO = \frac{heave\ amplitude}{wave\ amplitude} = \frac{2 \times heave\ amplitude}{2 \times wave\ amplitude} = \frac{heave\ height}{wave\ height} \quad (4)$$

3.5. Mathematical model of the device

In order to derive a simplified mathematical model of the proposed WEC the following assumptions were made:

- The device (a point absorber) is constrained to oscillate only in the vertical direction, and therefore will have a linear response (Das & Baghfalaki, 2014).
- The floating body has lateral symmetry (Das & Baghfalaki, 2014).
- The incident wave is sinusoidal (Das & Baghfalaki, 2014).

The response of the system can be compared to that of a typical spring-mass-damping system (Figure 38), subjected to an external force (F_E) in the direction of the z-axis.

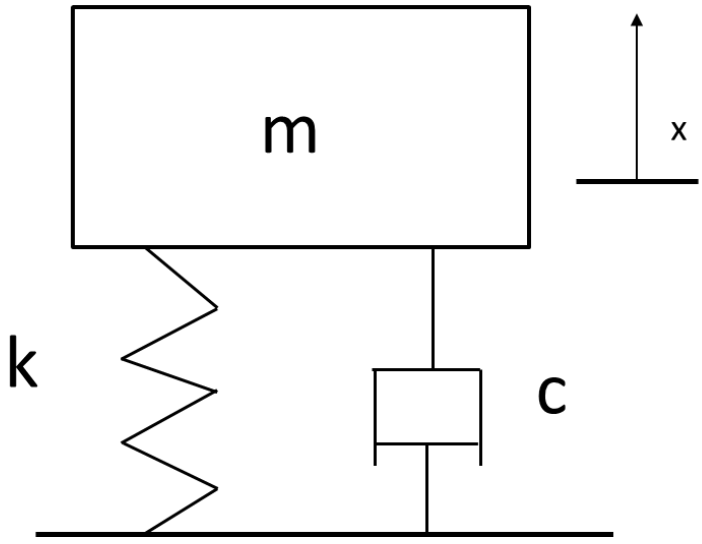

Figure 38. Spring mass-damping system.

According to Newton's Second Law, the system can be expressed as:

$$m\ddot{x} = \sum F = -F_k - F_c + F_E \quad (5)$$

where $m\ddot{x}$ is the inertia force, $\sum F$ is the resultant force, F_E is the external force acted on the system, and F_c is the damping force which be defined further as $F_c = c\dot{x}$ where c is the damping coefficient and $\dot{x}$ represents the velocity. (Yin & Technology Press, 2013).

Therefore Equation 5 can be rewritten as:

$$m\ddot{x} + c\dot{x} + kx = F_E \quad (6)$$

When applied to the scale model the parameters of Equation 6 are defined as (Yin & Technology Press, 2013):

m = mass of buoy or the total mass of buoy and ballast

c = damping coefficient

k = constant of spring under hydrostatic buoyancy condition

An important feature of the system is the natural or resonant frequency, f_0, the frequency which produces the maximum amplitude on the floating body (in the case of the point absorber the floating body is the buoy). Moreover, the highest efficiency of absorption for a point absorber can be achieved when the frequency of the incident wave is equal to the resonant frequency (Yin & Technology Press, 2013).

$$f_o = \frac{1}{2\pi}\sqrt{\frac{k}{m}} \quad (7)$$

If the device is under the condition of still water, F_E would be zero (Yin & Technology Press, 2013) and Equation 6 can be expressed as:

$$m\ddot{x} + c\dot{x} + kx = 0 \quad (6a)$$

The solution to Equation 6a can be assumed to be a system of differential equations (Equations 8a – 8c) (Singiresu, 1995; Yimin, 2007).

$$x(t) = e^{st} \quad (8a)$$

$$\dot{x}(t) = se^{st} \quad (8b)$$

$$\ddot{x}(t) = s^2e^{st} \quad (8c)$$

where s is a constant.

Inserting $x(t)$, $\dot{x}(t)$ and $\ddot{x}(t)$ into Equation 6, a characteristic equation is given:

$$ms^2 + cs + k = 0 \quad (9)$$

$$s_{1,2} = \frac{-c\pm\sqrt{bc^2 - 4mk}}{2m} = -\frac{c}{2m} \pm \sqrt{\left(\frac{C}{2m}\right)^2 - \frac{k}{m}} \quad (10)$$

Thus, the general solution of differential Equation (6a) is

$$x(t) = C_1 e^{s_1 t} + C_2 e^{s_2 t} = C_1 e^{\left(-\frac{c}{2m} \pm \sqrt{\left(\frac{c}{2m}\right)^2 - \frac{k}{m}}\right)t} + C_2 e^{\left(-\frac{c}{2m} \pm \sqrt{\left(\frac{c}{2m}\right)^2 - \frac{k}{m}}\right)t} \quad (11)$$

where the C_1 and C_2 are arbitrary constants which can be determined from the initial motion conditions of system (Singiresu, 1995).

The critical damping, denoted by c_c, comes from the value when the damping constant c in Equation 10 equals to zero (Singiresu, 1995):

$$\left(\frac{c_c}{2m}\right)^2 - \frac{k}{m} = 0$$

$$c_c = 2m\sqrt{\frac{k}{m}} = 2\sqrt{km} = 2m\omega_n \quad (12)$$

where the ω_n is the circular natural frequency, which is expressed as:

$$\omega_n = \sqrt{\frac{k}{m}} \quad (13)$$

The definition of damping ratio ζ is the ratio of the damping constant to the critical damping constant (Singiresu, 1995).

$$\zeta = \frac{c}{c_c} = \frac{c}{2\sqrt{km}} = \frac{c}{2m\omega_n} \quad (14)$$

Thus, Equation 6a can be rewritten as:

$$\ddot{x} + 2\zeta\omega_n\dot{x} + \omega_n^2 x = 0 \quad (15)$$

The characteristic equation can also be expressed as:

$$s^2 + 2\zeta\omega_n s + \omega_n^2 = 0 \quad (16)$$

The nature roots s_1 and s_2 are given by:

$$s_{1,2} = -\zeta\omega_n \pm \omega_n\sqrt{\zeta^2-1} \quad (17)$$

The solution of Equation 11 can be rewritten as:

$$x(t) = C_1 e^{(-\zeta\omega_n + \omega_n\sqrt{\zeta^2-1})t} + C_2 e^{(-\zeta\omega_n - \omega_n\sqrt{\zeta^2-1})t} \quad (18)$$

For the roots of characteristic equation, three cases, which are $\zeta<1$, $\zeta=1$ and $\zeta>1$, will be discussed respectively (Yimin, 2007).

Case 1. Underdamped system ($\zeta<1$)

For this case, $\zeta^2 - 1$ is negative and the roots $s_{1,2}$ can be expressed as:

$$s_{1,2} = -\zeta\omega_n \pm i\sqrt{1-\zeta^2}\omega_n \quad (19)$$

where i equals to $\sqrt{-1}$ (Yimin, 2007). Hence, the solution of Equation 18 is rewritten as:

$$x(t) = e^{-\zeta\omega_n t}\left(C_1 e^{i\sqrt{1-\zeta^2}\omega_n t} + C_1 e^{-i\sqrt{1-\zeta^2}\omega_n t}\right) \quad (20)$$

The derivative of Equation 20 is:

$$\dot{x} = -\zeta\omega_n e^{-\zeta\omega_n t}(C_1 e^{i\omega_d t} + C_1 e^{-i\omega_d t}) + -\zeta\omega_n e^{-\zeta\omega_n t}(C_1 e^{i\omega_d t} - C_1 e^{i\omega_d t}) \quad (21)$$

By using the initial conditions t = 0, $x = x_0$ and $\dot{x} = \dot{x}_0$

$x_0 = C_1 + C_2$, $\dot{x}_0 = -\zeta\omega_n(C_1 + C_2) + i\omega_d(C_1 - C_2)$

and

$C_1 = \frac{\dot{x}_0 + (\zeta\omega_n + i\omega_d)x_0}{i2\omega_d}$, $C_1 = \frac{-\dot{x}_0 + (-\zeta\omega_n + i\omega_d)x_0}{i2\omega_d}$

According to the Euler Equation, $e^{\pm i\omega_d t} = cos i\omega_d t \pm i sin\omega_d t$ (Yimin, 2007), Equation 20 can be rewritten as:

$$x = e^{-\zeta\omega_n t}(C_1 cos\omega_d t + C_2 sin\omega_d t) \quad (22)$$

The C_1 and C_2 can be solved by the initial conditions that t=0, $x=x_0$, $\dot{x}= \dot{x}_0$.

$C_1=x_0$, $C_2= (\dot{x}_0+ \zeta\omega_n x_0)/ \omega_d$

Using trigonometric function transformations (Yimin, 2007), let $C_1= A\sin\varphi$ and $C_2 = A\cos\varphi$ the Equation 22 will become:

$$x = Ae^{-\zeta\omega_n t}\sin(\omega_d t + \varphi) \quad (23)$$

In Equation 23, A and φ are undetermined constants, and they are also able to be determined by the initial conditions, which t=0, $x=x_0$, $\dot{x}= \dot{x}_0$

$$A = \sqrt{{x_0}^2 + \left(\frac{\dot{x}_0+\zeta\omega_n x_0}{\omega_d}\right)^2}, \tan\varphi = \frac{\omega_d x_0}{\dot{x}_0+\zeta\omega_n x_0} \quad (24)$$

where ω_d is the frequency of damped vibration, and the function of that can be expressed as:

$$\omega_d = \sqrt{1-\zeta^2}\omega_n \quad (25)$$

It is clear that the frequency of damped vibration ω_d is less than the undamped natural frequency ω_n. The undamped case is one of the typical models to lead to an oscillating motion (Singiresu, 1995).

The plot of Equation 23 is showed in Figure 39, which illustrates the relationship about period and amplitude.

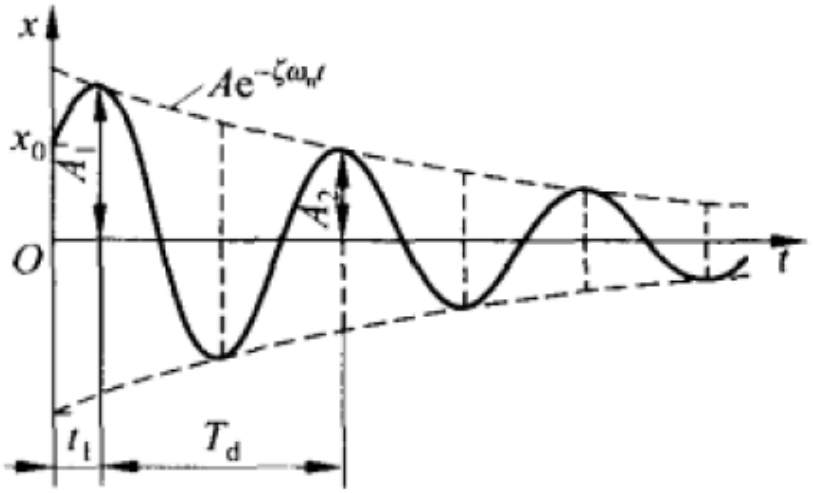

Figure 39. Plot of damped system using Equation 23 (Yimin, 2007).

It can be seen that the plot is limited between the curve of $Ae^{-\zeta\omega_n t}$, and is not simple harmonic vibration with the equal amplitude. For this case, damping performances two properties for the vibration system (Yimin, 2007).

First of all, T_d is the period of this response of vibration system which is time between two successive peaks, such as A_1, A_2 in plot. T_d can be expressed as:

$$T_d = \frac{2\pi}{\omega_d} = \frac{2\pi}{\sqrt{1-\zeta^2}\omega_n} = \frac{1}{\sqrt{1-\zeta^2}}T \tag{26}$$

$$f_d = \frac{\omega_d}{2\pi} = \sqrt{1-\zeta^2}f \tag{27}$$

where T and f is the period and frequency of free vibration without damping. The period increased but decreased in frequency by damping effect. Moreover, when the value of damping ratio, ζ, is small, the influence of damping ratio on system can be neglected (Yimin, 2007).

Secondly, damping ratio makes response of system be a decrement of geometric progression in amplitude. The ratio of adjacent amplitude, which is also the ratio

of the displacements measured a period apart, can be given as (Bottega, 2014):

$$\frac{x_1}{x_2} = \frac{Ae^{-\zeta\omega_n t}}{Ae^{-\zeta\omega_n (t-T_d)}} = e^{\zeta\omega_n T_d} \tag{28}$$

This ratio is also expressed by the logarithmic decrement, δ, which is defined as the natural log of the ratio of the two successive adjacent amplitudes (Bottega, 2014). The logarithmic decrement, δ, can be given as:

$$\delta = \ln\frac{x_1}{x_2} = \ln e^{\zeta\omega_n T_d} = \zeta\omega_n T_d = \frac{2\pi\zeta}{\sqrt{1-\zeta^2}} \tag{29}$$

hence the damping ratio can be determined from Equation 29 to give:

$$\zeta = \frac{\delta}{\sqrt{4\pi^2+\delta^2}} \tag{30}$$

If $\zeta \ll 1$, Equation 30 can be rewritten as:

$$\zeta \approx \frac{\delta}{2\pi} \tag{31}$$

For the successive instants during the time, a natural period on the displacement produces the interval of adjacent instants (Bottega, 2014). The relationship ratio of the first and last measurements is given as:

$$\frac{x_1}{x_2} = \frac{x_2}{x_3} = \cdots = \frac{x_n}{x_{n+1}} = e^{\zeta\omega_n T_d} \tag{32}$$

$$\frac{x_1}{x_{n+1}} = \left(\frac{x_1}{x_2}\right)\left(\frac{x_2}{x_3}\right)\cdots\left(\frac{x_n}{x_{n+1}}\right) = e^{n\delta} \quad (33)$$

$$\delta = \frac{1}{n}\ln\frac{x_1}{x_{n+1}} \quad (34)$$

Case 2: Critically damped system (ζ=1)

In this case, the magnitude of amplitude of system is going to zero which is can be seen in Figure 40 with various result curves, and the characteristic equation has two real and equal roots (Yimin, 2007). The roots are given:

$s_{1,2} = -\zeta\omega_n = -\omega_n \quad (35)$

and the general solution is:

$$x = (C1 + C2t)e^{\zeta\omega_n t} \quad (36)$$

substitute initial conditions, $x(0) = x_0$ and $\dot{x}(0) = v_0$

$$x = [x_0 + (\dot{x_0} + \omega_n x_0)t]\, e^{\omega_n t} \quad (37)$$

It is can be seen that Equation 37 is a response of exponential decrement, $\dot{x_0}$ is able to determine different results by curves which are displayed in Figure 40.

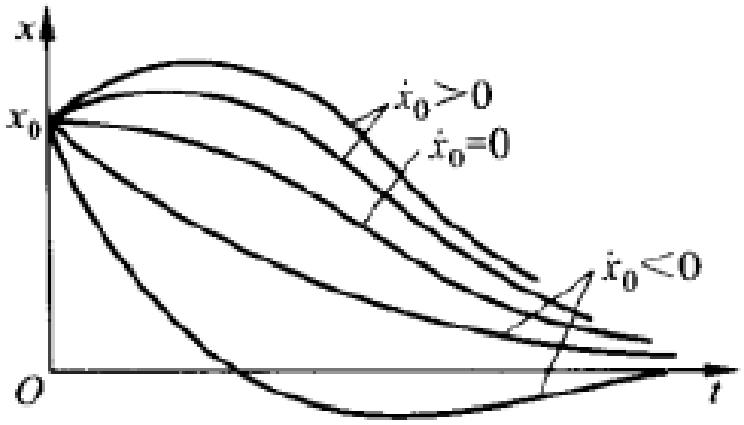

Figure 40. Characteristic response of critically damped systems (Yimin, 2007).

Case 3 Overdamped system (ζ>1)

In overdamped system case, the motion of system will diminish gradually to zero for amplitude without oscillating, which is displayed in Figure 41. The characteristic equation has two real and distinct roots (Singiresu, 1995) and are given by:

$$s_{1,2} = (-\zeta \pm \sqrt{\zeta^2 - 1})\omega_n \quad (38)$$

hence the solution is able to be given as:

$$x(t) = C_1 e^{(-\zeta\omega_n + \omega_n\sqrt{\zeta^2-1})t} + C_2 e^{(-\zeta\omega_n - \omega_n\sqrt{\zeta^2-1})t} \quad (39)$$

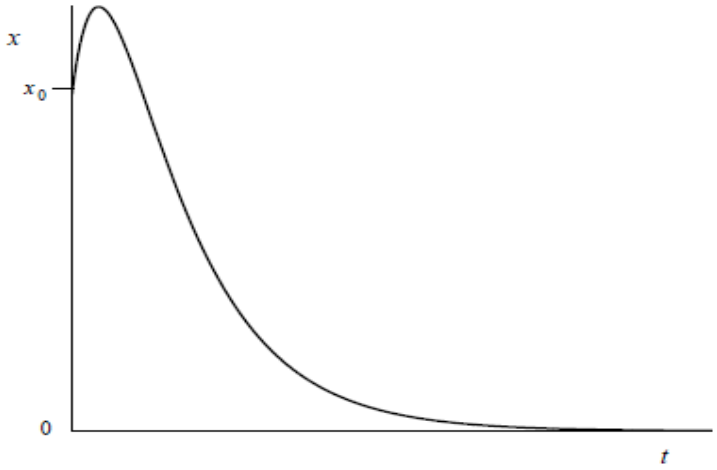

Figure 41. Characteristic response of overdamped system (Bottega, 2014).

For this model device, the device schematic is shown in Figure 42.

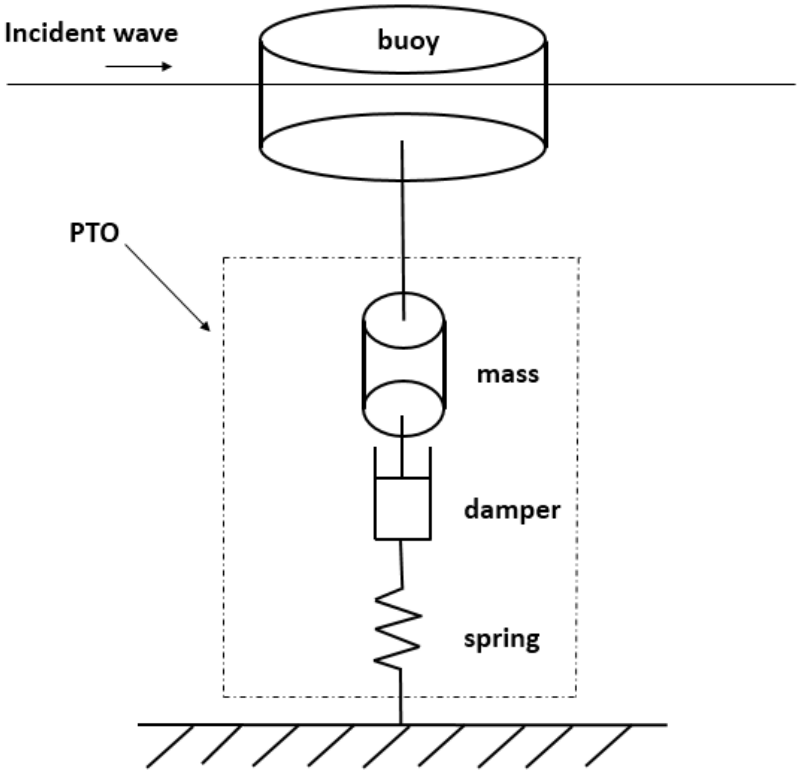

Figure 42. Schematic of model device.

The detailed natural frequency equation (Cheng, Yang, Hu, & Xiao, 2014) and parameters are:

$$\omega = \sqrt{\frac{\rho g A + K_{PTO}}{m + M + M_{PTO}}} \quad (40)$$

ρ: the water density

g: gravity acceleration

A: the section area of buoy

K_{PTO}: stiffness of PTO, the spring constant

m: mass of buoy

M: added mass

M_{PTO}: the total mass of PTO

The added mass is the added effect from the flow around underwater bodies, and this effect must be considered due to the fluid acts on the marine bodies (Fackrell, 2011). The equation can be expressed as:

$$M_{add} = \frac{\pi d^2 L}{4} \rho \quad (41)$$

where the d is the diameter of buoy, and L is the height of buoy.

The result of the added mass, M_{add}, is 0.628 kg.

3.6. Summary

This chapter has described the preparation of investigation of the model device, including detailed setup, aims, mathematical theory and method of data analysis. The procedures of each test are also explained step by step. The next chapter will present and discuss the results of the experimental work.

4. Results and Discussion

This chapter presents the result and discussion of tests. For the still water case, a free response of device as an experimental test was conducted by different constant of spring in PTO, and the theoretical results were also calculated to do comparison. Irregular and regular wave tests were regard as forced response water tests of model device with PTO in different constant. The results of those were compared in amplitude, period and frequency by figures. Moreover, the RAO tests were also tested under the two PTO cases. The results of all tests are shown in tables and figures in order to make all things clear. The results and calculation were followed by the method and detailed equations from Chapter 3.

4.1. Free response of the system (Still water test)

4.1.1. Theoretical results

The theoretical natural frequency values for the two springs tested were calculated using the mathematical model derived in Section 3.5. The theoretical values of the softer (Spring 2) and stiffer (Spring 1) springs are presented in Table 7. The natural angular frequency for the two cases was calculated by using Equation 40, and thereafter the natural linear frequency and the corresponding natural period were calculated.

Table 7. Theoretical results for the natural frequency for the model device.

Spring	Parameter	Value
Soft (Spring 2)	natural angular frequency (rad/s)	13.398
	natural linear frequency (Hz)	2.132
	natural period (s)	0.468
Stiff (Spring 1)	Natural angular frequency (rad/s)	17.989
	natural linear frequency (Hz)	2.863
	natural period (s)	0.349

4.1.2. Experimental results

The theoretical motion of the device was assumed to be an underdamped vibration model, so therefore the expected behaviour was that of the system oscillating with gradually decreasing amplitudes. However, when the stillwater tests were undertaken for each spring (Spring 1 and 2), the buoy only one oscillated once. As a consequence, experimental results were unable to be obtained for the stillwater tests, so, therefore, it couldn't be compared with the theoretical values calculated in Section 4.1.1.

4.1.3. Discussion

The theoretical results for the motion of the model device illustrates the differences in natural frequency for each spring. As expected, the natural angular and linear frequency was greater for Spring 1 (the stiffer spring) compared to that of Spring 2 (the softer spring), and the inverse was true for the calculated natural periods. These results mean that if the PTO mechanism of device has a relatively high stiffness coefficient (i.e. high mass), the response of the buoy is faster and more sensitive with more oscillations thus generating more power for a real

device. In contrast, the PTO part with low stiffness coefficient (i.e. low mass) generates low buoy sensitivity in response to the incident wave motion with lower electricity production in real life. To this extent, the mass of PTO is a significant factor that determines the overall system performance.

An issue with the experimental device is that the seal around the connecting rod (the O-ring), was restricting the movement of the rod, as the fit was too tight. This was the lead cause of the buoy not being able to perform the successive oscillations in the stillwater tests.

However, the O-ring is a critical part of the design as it seals the chamber that houses the PTO from the highly corrosive marine environment. Therefore for this device there will be trade-offs between effective sealing and additional friction.

4.2. Forced response of the system

4.2.1. Results – Irregular wave tests

Figure 43, Figure 44, and Figure 45 illustrate the performance of the physical model for panchromatic wave conditions. The tests for panchromatic wave conditions were conducted following the procedures in Section 3.3.2.

Figure 43 illustrates the successive oscillations of the physical device when the PTO is modelled as the spring with the low spring constant (the softer spring). It can also be seen in this figure that the device does not return to its original position during the duration of the test. This is because the softer spring is easily driven by the buoy under the excitation force (the generated wave), which means the restoring force (the spring) is not stiff enough to pull the buoy back. As the excitation forces decrease (the waves are no longer being generated), the buoy's oscillations gradually reduce as the excitation forces become less than the restoring force.

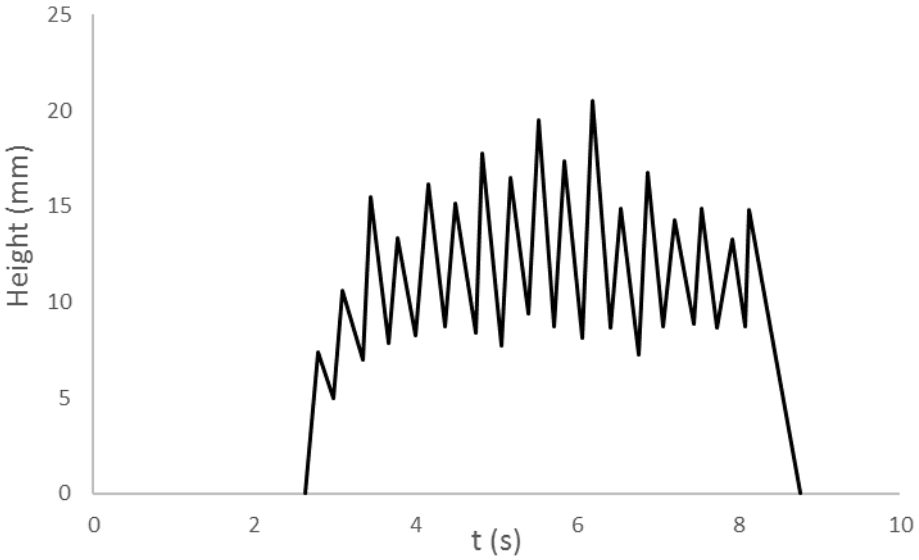

Figure 43. Oscillations of the physical model with the softer spring (low spring constant).

In contrast, when the PTO is modelled as the stiffer spring, the physical device returns to its original position after each oscillation (Figure 44). This is because the stiffer spring can provide enough restoring force to against excitation force.

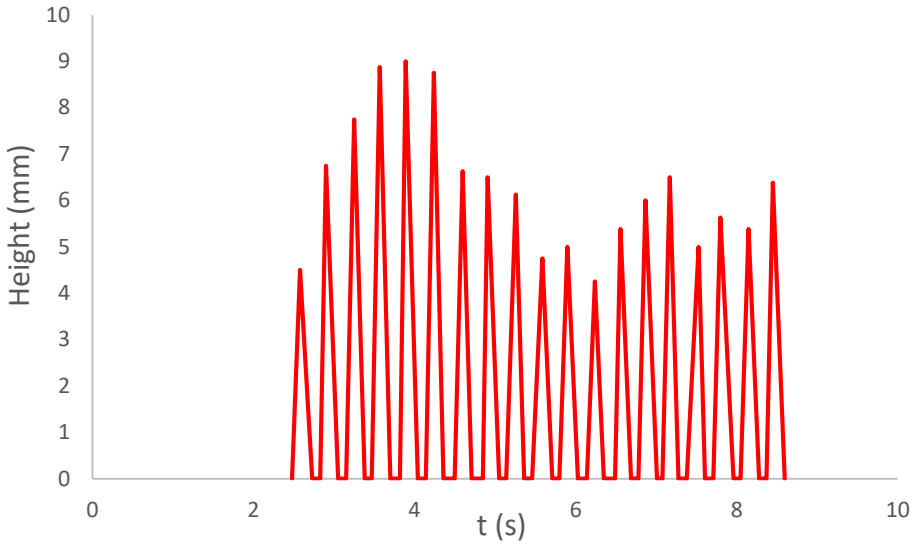

Figure 44. Oscillation of the physical model with the stiffer spring (high spring constant).

Figure 45 illustrates the comparison between the two cases where it is clear that the motion of the soft spring case is similar to the stiff spring case, although the soft spring did not return to the bottom of the device until the end of the test.

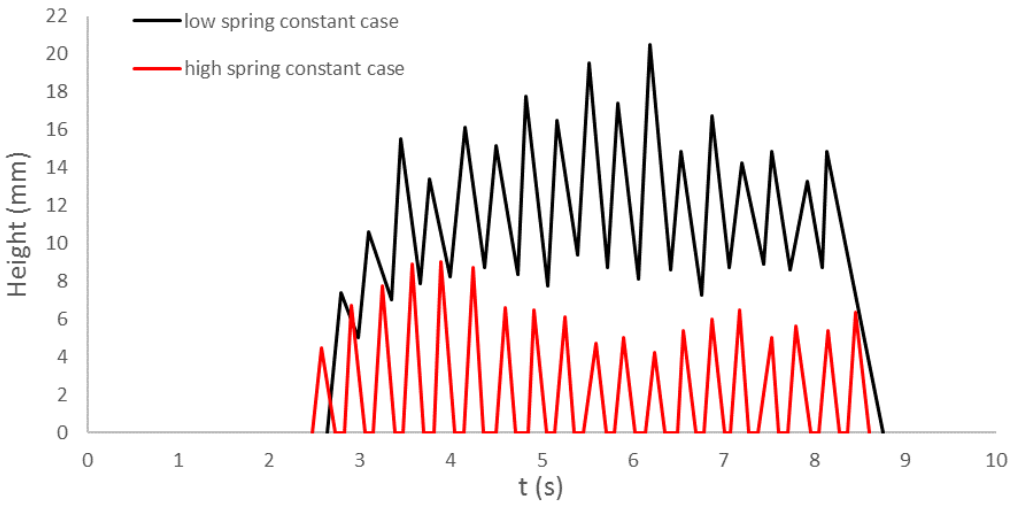

Figure 45. Comparison of the oscillations of the physical device for each spring.

The time interval between successive oscillations is presented in Figure 46, which clearly shows that the investigator generated random waves for both device iterations.

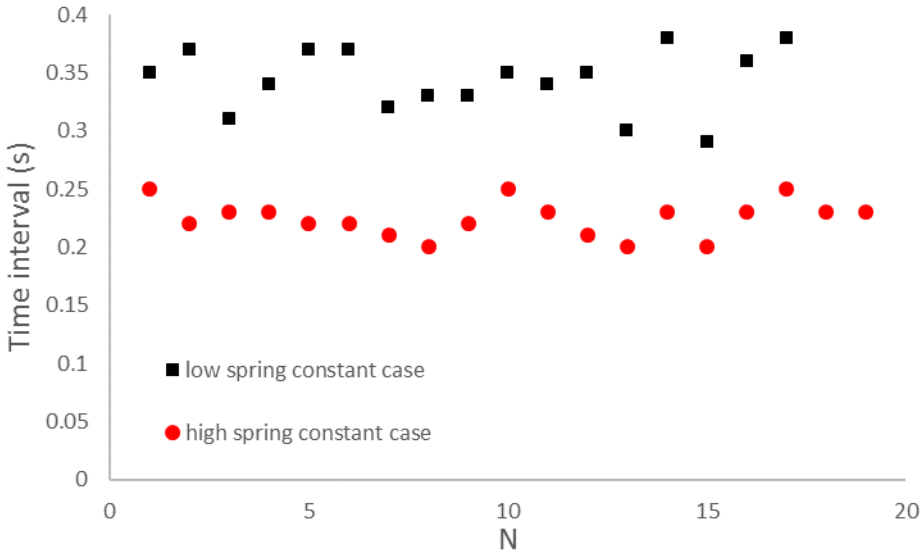

Figure 46. Time interval comparison for each device iteration.

4.2.2. Discussion – Irregular wave tests

As seen in Figure 43, Figure 44, and Figure 45, the physical device reacts differently for the two different springs used to model the PTO mechanism. The low spring constant spring (the softer spring) has a greater response to the incoming waves (the excitation force) then the higher spring constant spring (the stiffer spring). Inversely this also means that the softer spring does not return to its original position during the test as unlike the stiffer spring, the restoring force is less than the external excitation force.

4.2.3. Results – Regular wave tests

In this section, the results of the tests subjected to monochromatic wave conditions are presented. This experiment is different from the irregular test as the waves generated have a single period (frequency) for the duration of the test. Regular tests were conducted for both iterations of the proposed device for a range of periods, per the procedure outlined in Section 3.3.2. The results presented in this section are for a two-second wave.

As seen in Figure 48 and Figure 49, the device exhibits cyclic behaviour due to the cyclic behaviour of the generated wave. The first iteration of the device, the softer spring, behaves similarly to that of the softer spring subjected to the irregular wave tests; the device does not return to its original position until the conclusion of the test run. The second iteration of the device, the stiffer spring, also behaves similarly to that of the stiffer spring subjected to the irregular tests; the device returns to its original position after each oscillation. In the regular tests, both iterations of the device experienced a series of regularly decreased motion for approximately two seconds between oscillations.

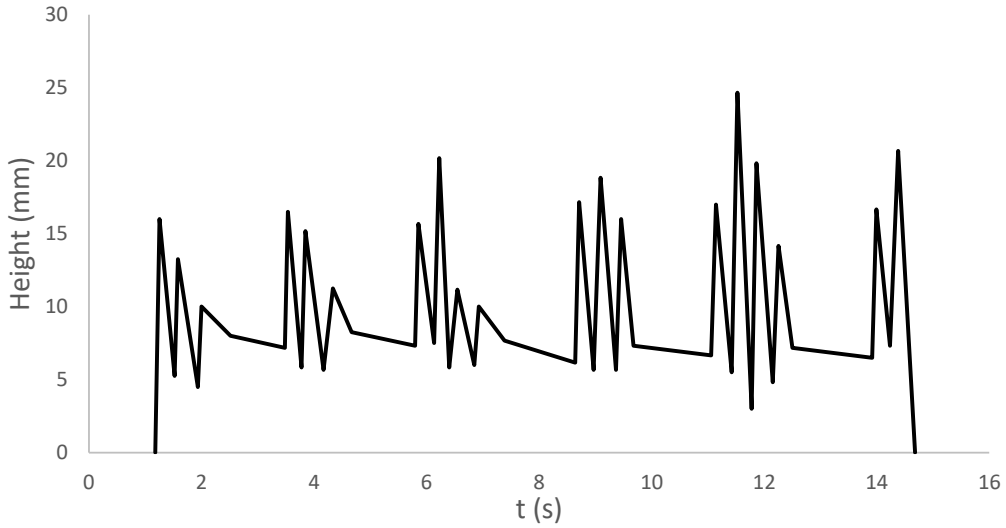

Figure 47. Oscillations of the physical model with the softer spring (low spring constant).

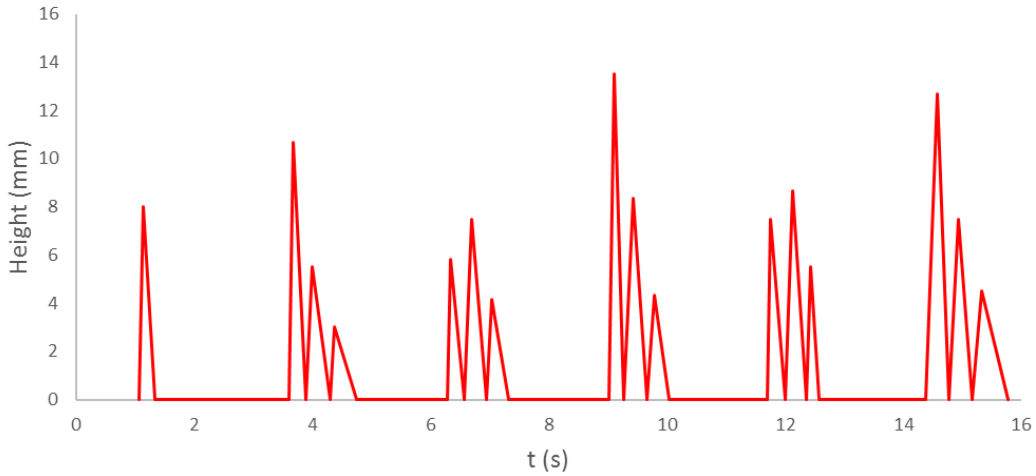

Figure 48. Oscillation of the physical model with the stiffer spring (high spring constant).

The comparison of the two cases (Figure 49) demonstrates the response of the physical device under the two PTO mechanisms (the soft and stiff springs). As seen in Figure 49 the response of the device for both iterations are matched during the same time interval, and as expected the response of the softer spring is greater than that of the stiff spring for the same excitation force.

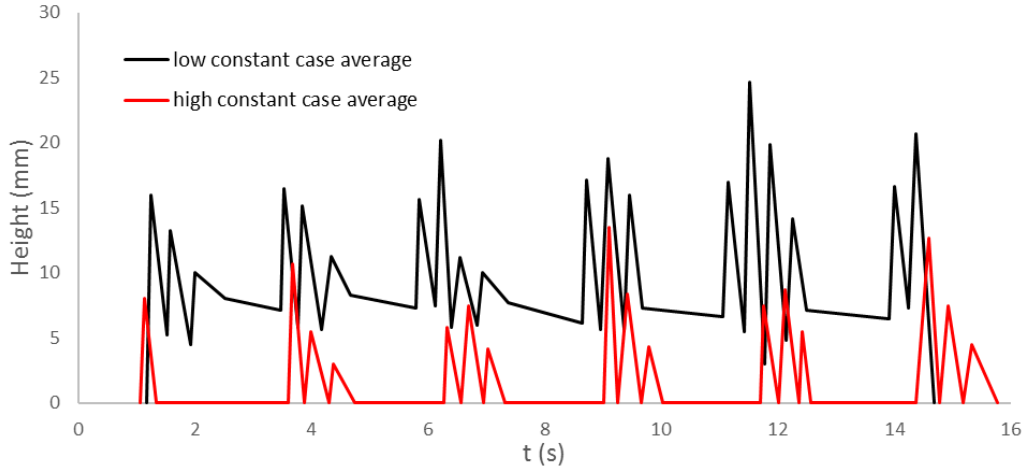

Figure 49. Comparison of the oscillations of the physical devise for each spring.

4.2.4. Discussion – Regular wave test

The behaviour of the device in the regular tests is similar to that demonstrated in the irregular tests, as the stiffness of the springs directly influences the restoring force of the device in response to the excitation force (the wave). For the softer spring, the WEC does not return to its original position until the end of the test. Whereas the stiffer spring results in the WEC returning to its original position after each oscillation. The softer spring also results in a greater response to the excitation force compared to that of the stiffer spring as seen in Figure 49.

4.3. Response Amplitude Operators

4.3.1. Results

The RAO values were calculated from the raw data obtained from the regular test video footage. Seven regular tests were conducted in total for each device iteration, where the average device height and the wave height was determined for each of these test runs. These values were utilised to calculate the RAO values (Equation 4) corresponding to the specific period (frequency) for that test run. The RAO values determined for each of the test runs for both device iterations (softer and stiffer springs) are depicted in Figure 50 and Figure 51. A comparison of the

softer and stiffer spring RAO curves are depicted in Figure 52.

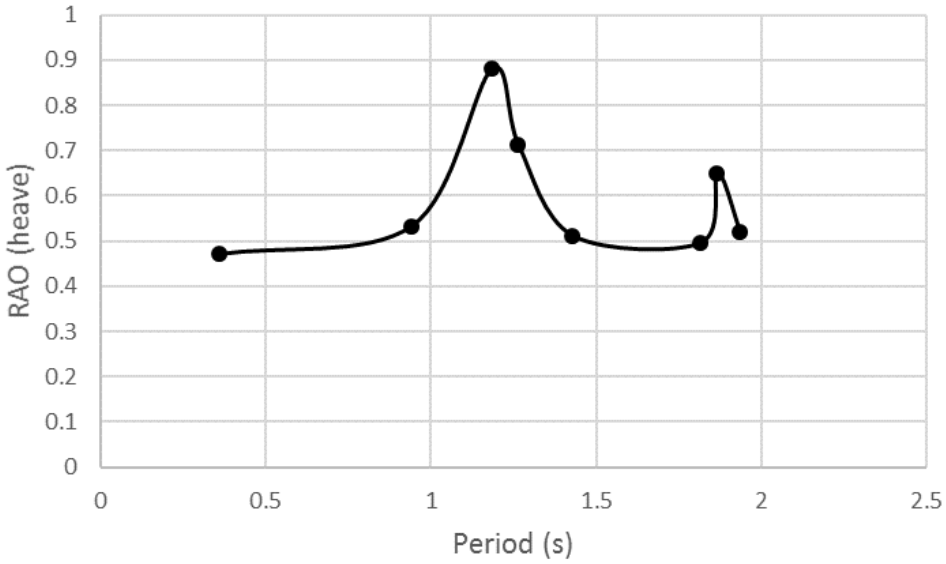

Figure 50. RAO results for soft spring.

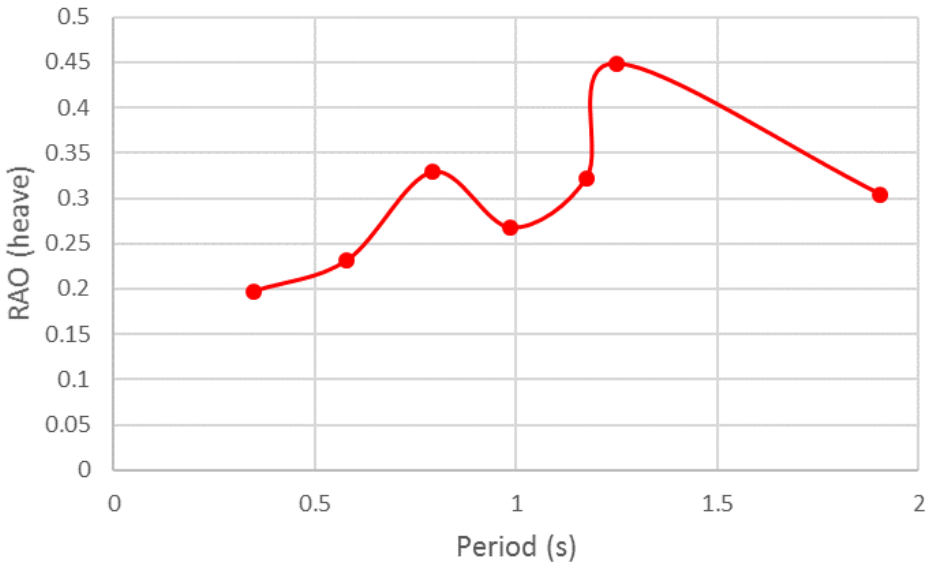

Figure 51. RAO results with stiff spring.

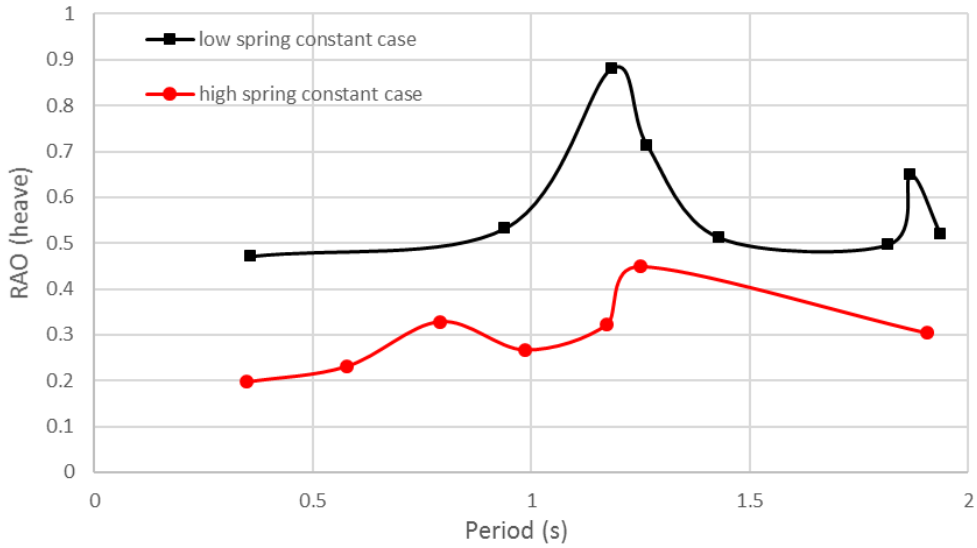

Figure 52. RAO comparison between the two springs.

4.3.2. Discussion

As predicted by the theory, the RAO value of softer spring case is much higher than that of the stiffer spring case, and both curves peaked at periods between 1 to 1.5 seconds. According to the definition of RAO, which is the ratio of the buoy heave displacement and wave height, the device could get the highest efficiency in energy conversion during this period.

The corresponding period of the highest point on each RAO curve is also the natural period of the device in heave, which is 1.18 seconds for the softer spring case, and 1.25 seconds for the stiffer spring case. Compared to the theoretical natural periods of the device calculated for the two spring cases in Section 4.1, the natural periods determined from the RAO curves are greater in both cases. This discrepancy between the results could be due to the additional stress between the rod and O-ring, as well as the pressure in the tube due to the oscillatory motion.

4.4. Wave Resource Assessment

A wave resource assessment of two sites off the coast of New Zealand will be undertaken in this section. Two sea areas of New Zealand were investigated

respectively and one site selected off the west coast of Auckland located in the North Island, and the second site off the south coast near Invercargill in the South Island. The location of the two sites are shown in Figure 53 and detailed maps of the two sites are shown in Figure 54 for the Auckland site and Figure 55 for the Invercargill site. The sea area coordinates of Auckland case is 37.1 S, 174.2 E with a depth of 91 m, and the Invercargill case is located at 46.8 S, 167.3 E with a depth of 150 m. Further details of the two sites including distance to the nearest port are given in Table 8.

The wave resource assessment presented was based on wave data over a 20 year from 1993 to 2012. The power density estimation of two sea areas was conducted by season and annually and averaged over the 20 year period. The wave data was provided by Danielle Bertram, a PhD student in the School of Engineering at the University of Waikato. The overall procedure for wave resource assessment is reviewed in Section 2.9.

The estimated mean available power for each season (summer, autumn, winter, and spring) for the Auckland site is shown in Figure 56. The results are presented by occurrences in plots. The figures plot H_{m0} (significant wave height) and T_e (energy wave period) and the value shown within the represents the power percentage or the percentage of the time that condition occurs. The power flux is calculated using Equation 1. The annual mean available power for the Auckland site is shown in Figure 57.

The estimated mean available power for each season for the Invercargill site is shown in Figure 58 and annually in Figure 59.

Figure 53. Map of New Zealand indicating the Auckland and Invercargill sites.

Table 8. Detailed site information.

	Auckland	**Invercargill**
Coordinate	37.1 S, 174.2 E	46.8 S, 167.3 E
Depth	91 m	159 m
Significate wave height scale	1.5 – 3.5 m	1.5 – 6m
Energy wave period scale	8 – 12 s	8 – 12 s
Closest distance from coastline	26 km	59 km
Distance of the nearest port	218 km (New Plymouth)	82 km (Bluff))
Closest distance from Stewart Island	-	31 km

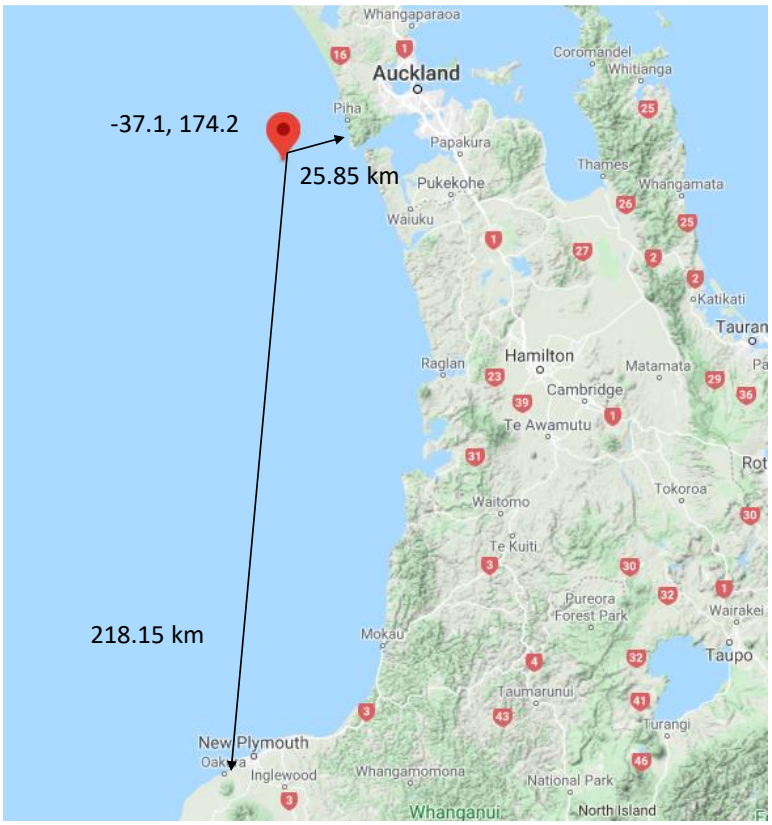

Figure 54. Detailed map of Auckland site.

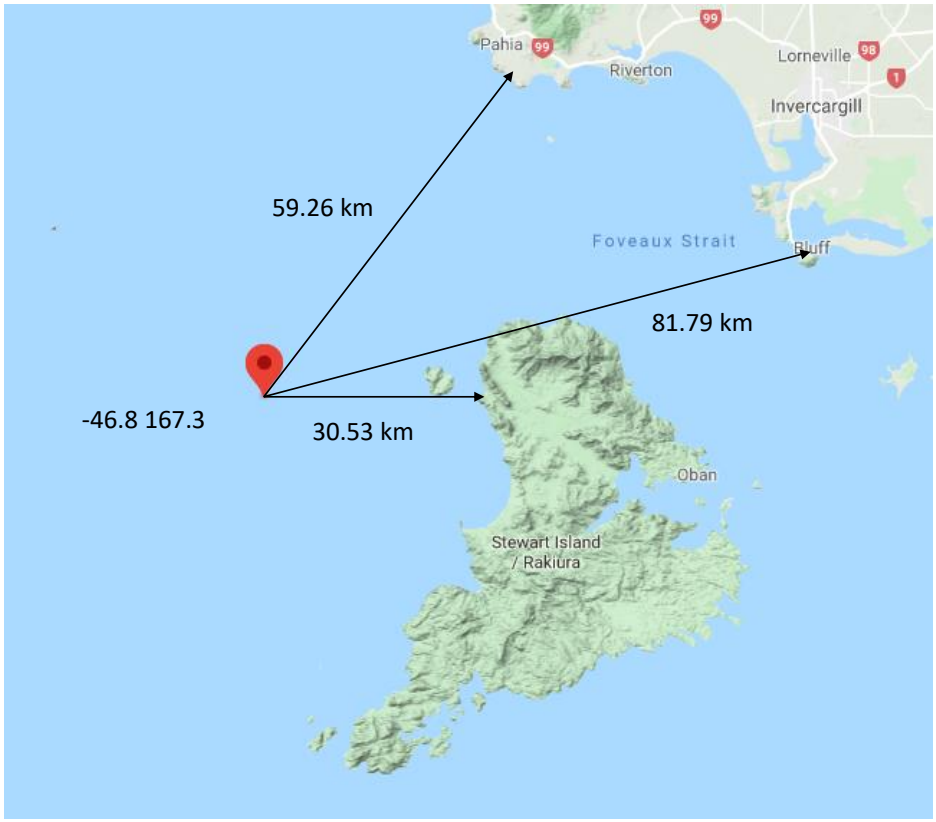

Figure 55. Detailed map of Invercargill site.

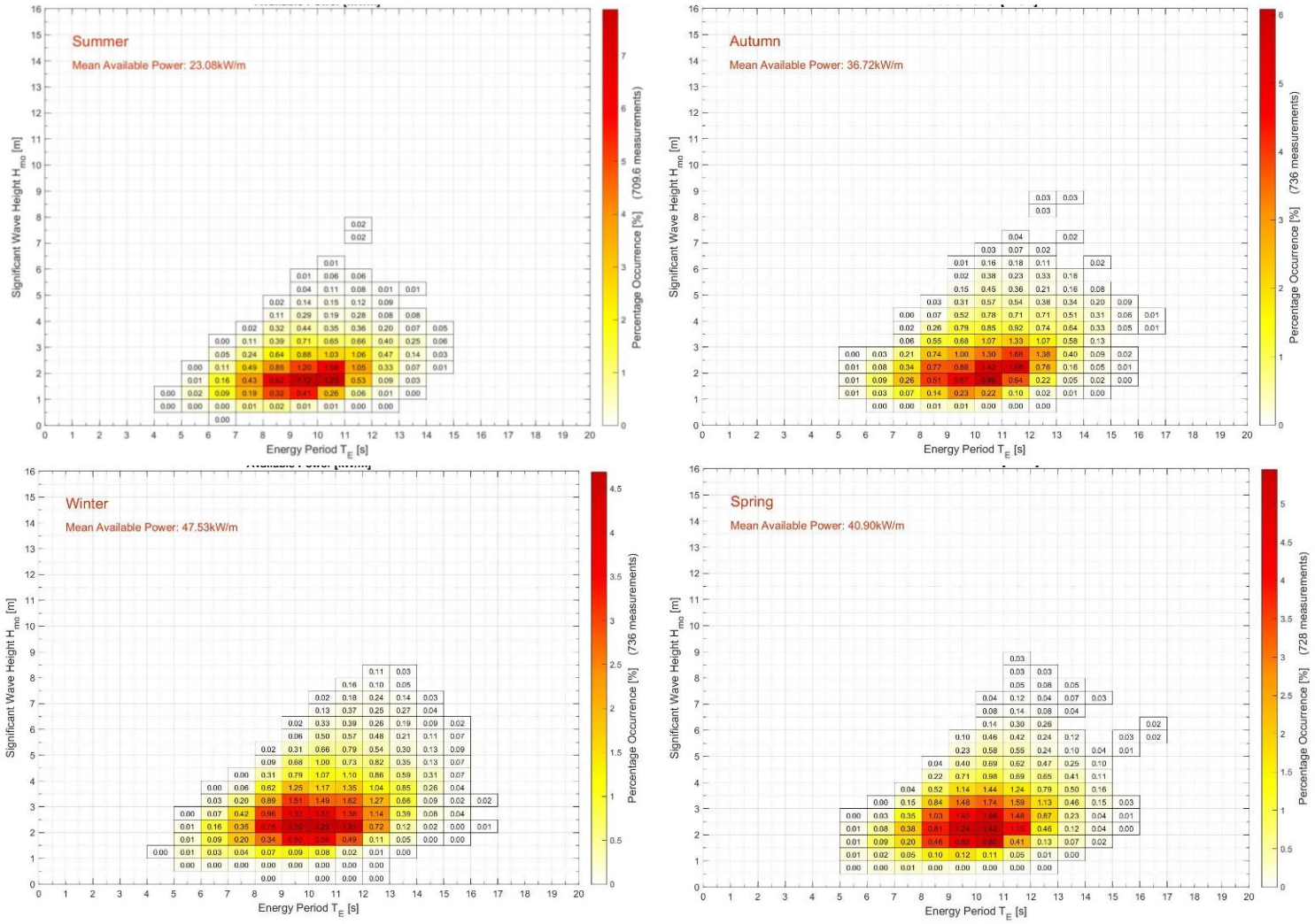

Figure 56. Seasonal mean available power for the Auckland site.

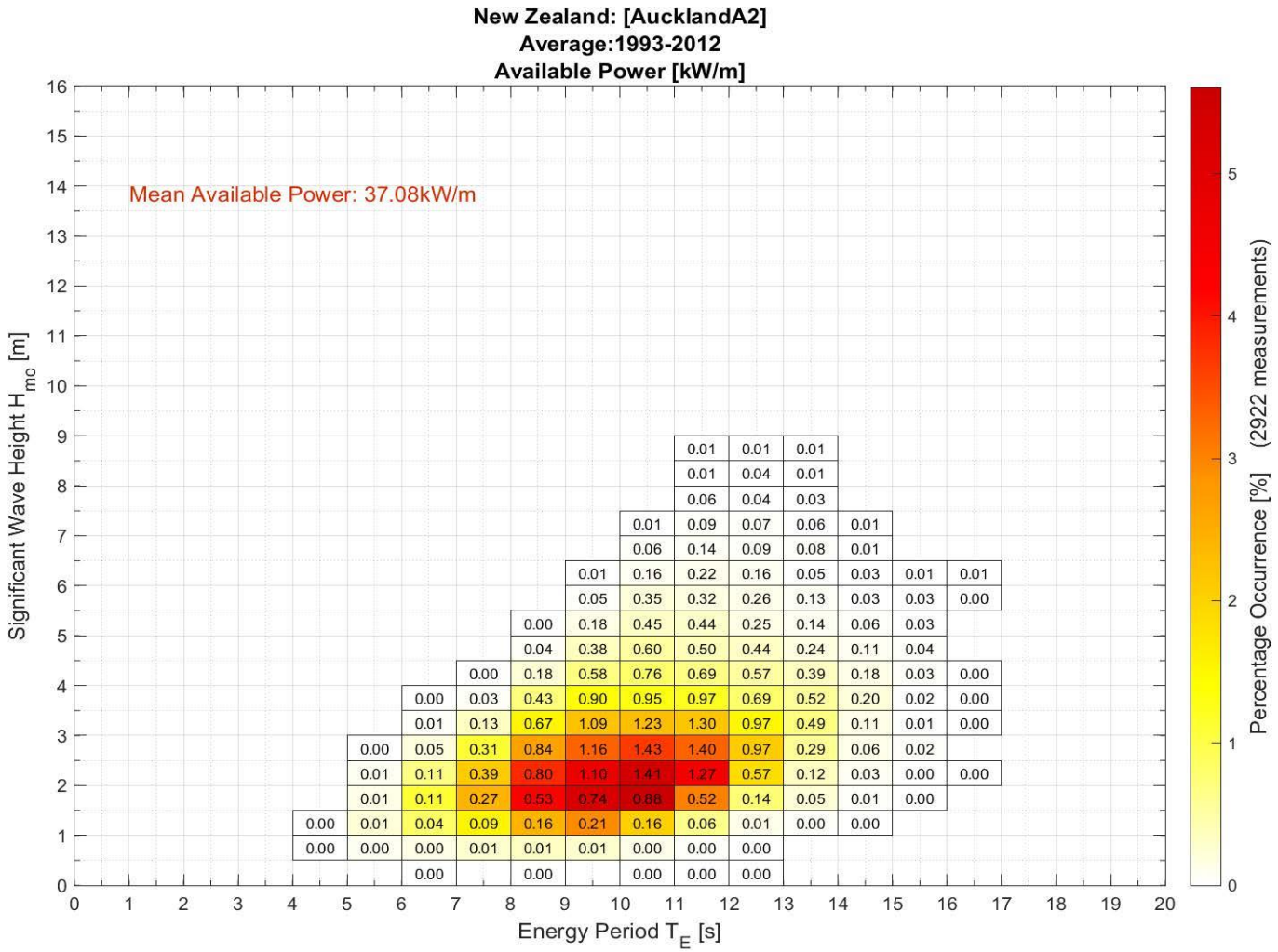

Figure 57. Annual mean available power for the Auckland site.

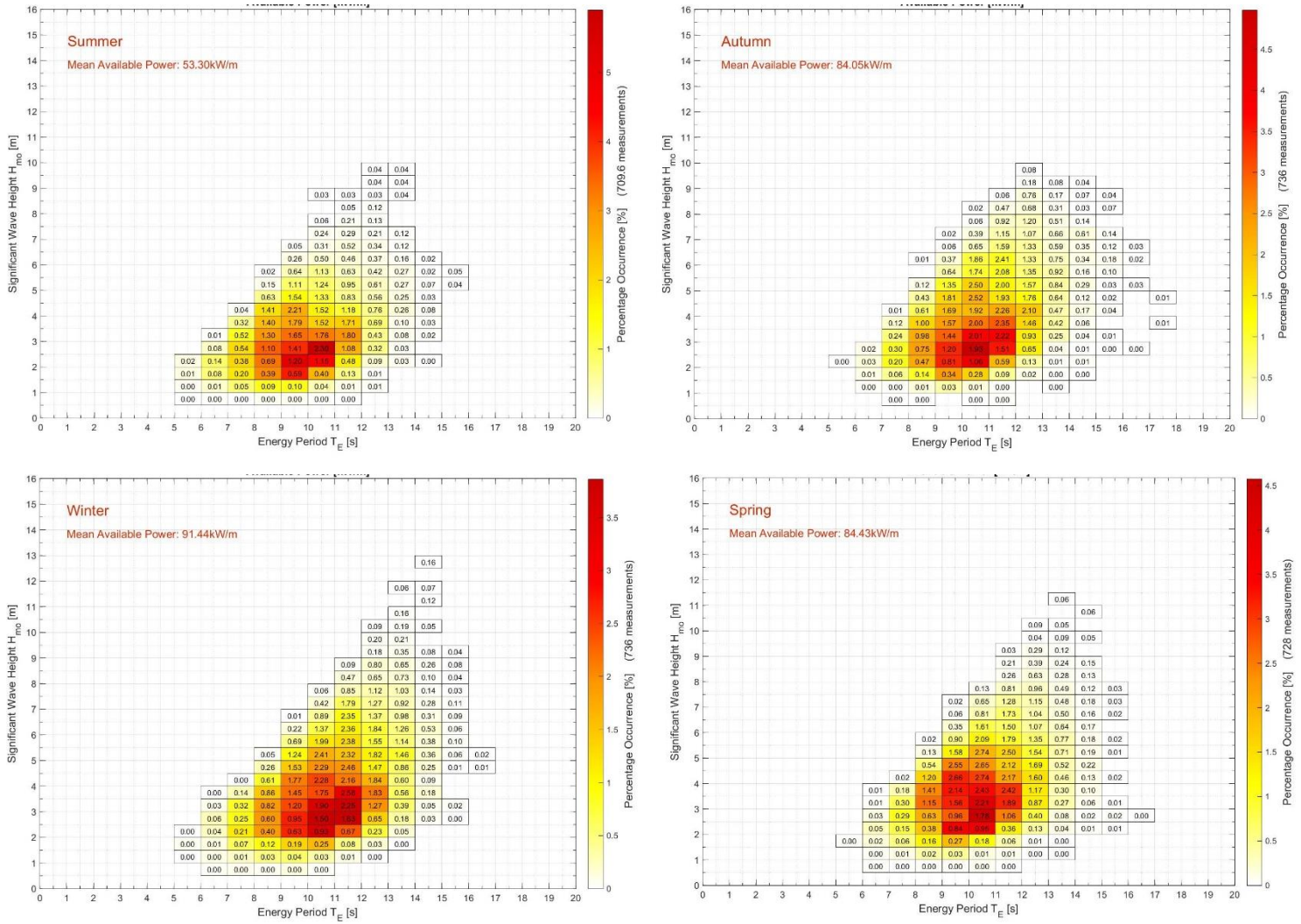

Figure 58. Seasonal mean available power for the Invercargill site

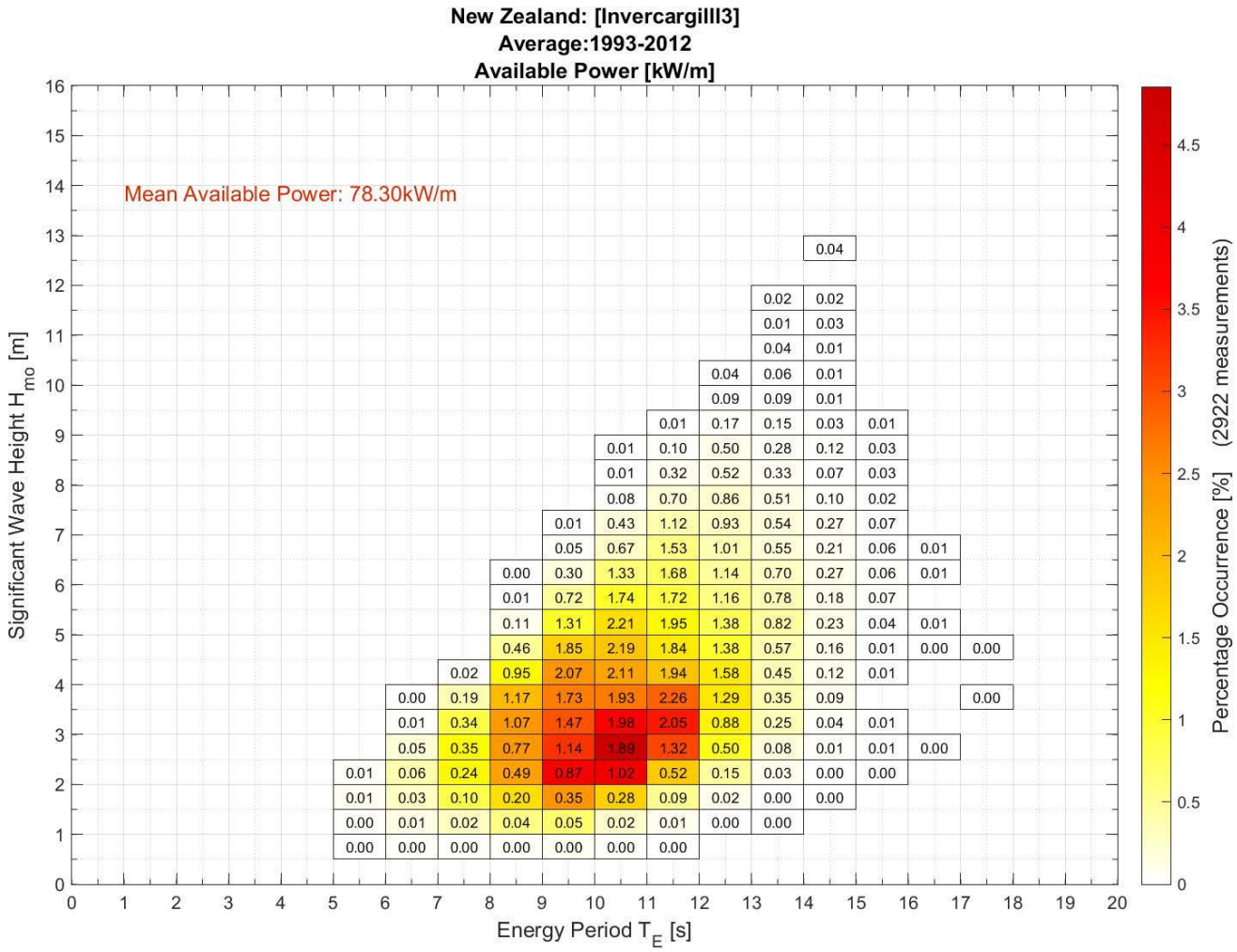

Figure 59. Annual mean available power for the Invercargill site.

According to 20-year variation plots for the Auckland site, it was clear that both spring and winter were over 40 kW/m in mean available power, with winter being 47.53 kW/m. By contrast summer and autumn was below 40 kW/m (summer = 23.06 kW/m). As can be seen from the values there is significant variation in mean available power between the seasons. The main power production was concentrated in the range of 8 to 12 seconds of the wave energy period with significant wave height between 1.5 m and 3.5 m. The mean annual available power for the Auckland site was 37.08 kW/m.

For the Invercargill site the H_{m0}-T_e scatter plots presented for the total mean available power level, the sea states with significant wave heights from 1.5 m to 6 m and energy period between 8 and 12 seconds have a considerable amount of available power. The seasons winter, spring and autumn had mean available power greater than 84 kW/m with the highest power flux of 91.44 kW/m occurring in winter. Similarly, to the Auckland site there was considerable variation between the seasons. The mean annual available power for the Auckland site was 78.30 kW/m.

4.4.1. Discussion – Comparison of sites

The results from the two sites are summarised in Figure 60 with variability by season and also annually. It is clear that the Invercargill site has a much greater potential than the Auckland site over all seasons. The Invercargill site would clearly be the most productive and promising site of the two, compared with the moderate sea area of Auckland.

Theoretically, power level at the greater latitude and higher wave heights are able to provide more available energy which is matched with the measured results shown in this section. In this wave resource assessment, both of sites has almost same wave energy period in scale between 8 to 12 seconds, which means the ideal natural period of practical point absorber devices should be in this scale in order to yield the greatest returns on investment. This is because in theory, the highest

efficiency of absorption for a point absorber can be achieved when the frequency of incident wave is equal to the frequency of resonant frequency.

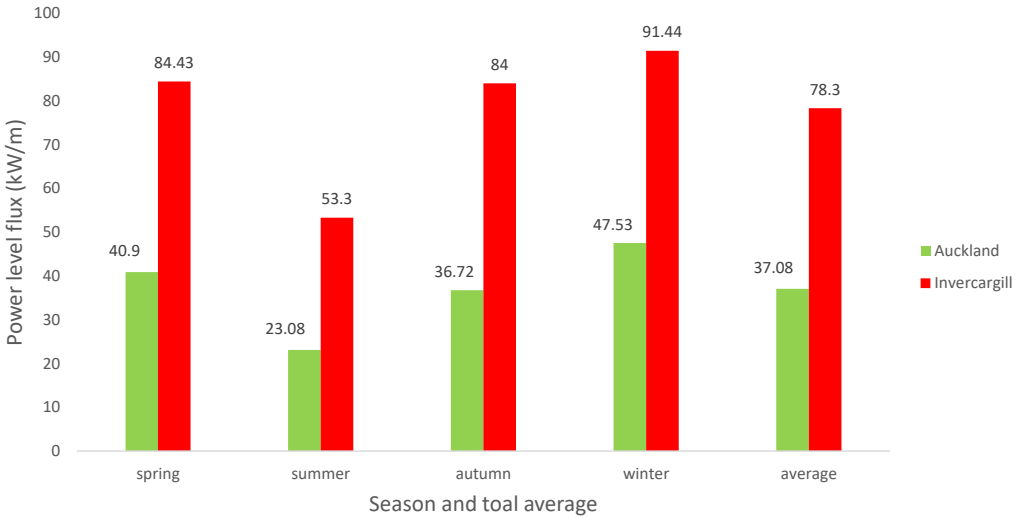

Figure 60. Comparison between the Auckland and Invercargill sites of power level flux by season.

The seasonal effects and geographic factors including latitudes, ocean currents also impact the available power level and energy harvest. Additionally, in the relatively high power density and long offshore area, a device can capture more energy from the high waves, but under extreme sea state and weather conditions, the devices have a high risk of damage so these factors must be considered to avoid damage to the device, improve the survivability of device and reduce maintenance costs so to maximise the working life of the device. Other considerations such as distance to shore, distance to closest port, and depth are also important considerations.

4.4.2. Summary

The main purpose of the experimental work was to determine the relationship between the performance of buoy motion and PTO portion of the device under irregular and regular wave conditions. For two conditions, the buoy response is much easier and more sensitive to the passing wave with a low stiffness PTO than

that of a PTO with high stiffness. However, the restoring force of the low stiffness PTO is less compared with the high stiffness PTO due to the different constant of springs. Moreover, the natural frequency/period was also determined from the mathematical model. Unfortunately, the stress generated from the relative motion of rod and O-ring and the tube pressure caused by the piston of PTO part were a potential influencing factor in the results.

The wave resource assessment is an important reference of a long-term estimation of power level and potential energy generation for a specific sea area. There is a large variation between seasons and also between sites as illustrated by the two New Zealand sites considered here.

5. Conclusions and Future Work

5.1.1. Conclusions

Wave energy is a promising although yet to be fully utilised source of energy for electricity generation. Numerous types of devices have been invested using different working principles. Point absorber WEC are promising devices that have started to be commercialised. The behaviour and performance of WEC is important to understand. The performance of the point absorber WEC model device considered in this work can be influenced by a number of factors. The stiffness of PTO is the one of the major effects that would affect device performance. The stiffness is mainly derived from the spring placed in PTO part. Under both regular and irregular wave conditions, the vertical displacement of PTO with lower stiffness is always higher than that of the stiffer case.

As predicted by the theory, the RAO value of softer spring case is much higher than that of the stiffer spring case, and both curves peaked at periods between 1 to 1.5 seconds. According to the definition of RAO, which is the ratio of the buoy heave displacement and wave height, the device could get the highest efficiency in energy conversion during this period.

The corresponding period of the highest point on each RAO curve is also the natural period of the device in heave, which is 1.18 seconds for the softer spring case, and 1.25 seconds for the stiffer spring case. Compared to the theoretical natural periods of the device calculated for the two spring cases, the natural periods determined from the RAO curves are greater in both cases. This discrepancy between the results could be due to the additional stress between the rod and O-ring, as well as the pressure in the tube due to the oscillatory motion.

In addition to the performance of the device, an assessment of the energy potential of specific sites is important to best match the device parameters with the resource. A wave resource assessment for two sites in New Zealand not only

provided a long-term estimate of available power but also a series of impact factor including season, currents and extreme sea states and potential requirements of design of point absorber device and other WECs. These detailed knowledge and information are important to get reliable economical and technical assessments of wave energy production.

5.1.2. Recommendations for future work

As with all experimental work there are limitations on the equipment and conditions that can be tested. The tests were limited to the equipment available, especially the size of the water tank and manual wave generation methods. A larger water tank with an automatic and controlled wave generator can improve the experimental results providing greater control and allowing a greater range of conditions to be tested. The number of tests conduction would be able to be increased more accurate data. Furthermore, using sensors and software algorithms to automatically record and track the motion of the buoy and PTO would also improve the accuracy of the data and provide a greater number of test conditions to be accomplished.

6. References

Aird, P. (2018). *Deepwater Drilling: Well Planning, Design, Engineering, Operations, and Technology Application*: Gulf Professional Publishing.

Al Shami, E., Wang, X., Zhang, R., & Zuo, L. (2019). A parameter study and optimization of two body wave energy converters. *Renewable energy, 131*, 1-13.

Al Shami, E., Zhang, R., & Wang, X. (2019). Point absorber wave energy harvesters: A review of recent developments. *Energies, 12*(1), 47.

Amiri, A., Panahi, R., & Radfar, S. (2016). Parametric study of two-body floating-point wave absorber. *Journal of Marine Science Application, 15*(1), 41-49.

Beatty, S. J., Hall, M., Buckham, B. J., Wild, P., & Bocking, B. (2015). Experimental and numerical comparisons of self-reacting point absorber wave energy converters in regular waves. *Ocean Engineering, 104*, 370-386.

Board, O. S., Council, N. R., Marine, & Committee, H. E. T. A. (2013). *An Evaluation of the US Department of Energy's Marine and Hydrokinetic Resource Assessments*: National Academies Press.

Bottega, W. J. (2014). *Engineering vibrations*: CRC Press.

Bull, D., & Ochs, M. E. (2013). Technological cost-reduction pathways for attenuator wave energy converters in the marine hydrokinetic environment. *Sandia National Laboratories*.

Chen, Z., Yu, H., Hu, M., Meng, G., & Wen, C. (2013). A review of offshore wave energy extraction system. *Advances in Mechanical Engineering, 5*, 623020.

Cheng, Z., Yang, J., Hu, Z., & Xiao, L. (2014). Frequency/time domain modeling of a direct drive point absorber wave energy converter. *Science China Physics, Mechanics Astronomy, 57*(2), 311-320.

Constans, J. (2013). *Marine Sources of Energy: Pergamon Policy Studies on Energy and Environment* (Vol. 53): Elsevier.

Czech, B., & Bauer, P. (2012). Wave energy converter concepts: Design challenges

and classification. *IEEE Industrial Electronics Magazine, 6*(2), 4-16.

Das, S. K., & Baghfalaki, M. (2014). Mathematical modelling of response amplitude operator for roll motion of a floating body: Analysis in frequency domain with numerical validation. *Journal of Marine Science Application, 13*(2), 143-157.

Drew, B., Plummer, A. R., & Sahinkaya, M. N. (2009). A review of wave energy converter technology. In: Sage Publications Sage UK: London, England.

Edenhofer, O., Pichs-Madruga, R., Sokona, Y., Seyboth, K., Kadner, S., Zwickel, T., . . . von Stechow, C. (2011). *Renewable energy sources and climate change mitigation: Special report of the intergovernmental panel on climate change*: Cambridge University Press.

Fackrell, S. (2011). *Study of the added mass of cylinders and spheres.* (PhD). University of Windsor, Ontario, Canada.

Fadaeenejad, M., Shamsipour, R., Rokni, S., & Gomes, C. (2014). New approaches in harnessing wave energy: With special attention to small islands. *Renewable Sustainable Energy Reviews, 29*, 345-354.

Falcão, A. F. J. I. S. T., Universidade Técnica de Lisboa. (2014). Modelling of wave energy conversion.

Garrison, T. S. (2012). *Essentials of oceanography*: Cengage Learning.

Göteman, M., Engström, J., Eriksson, M., Hann, M., Ransley, E., Greaves, D., & Leijon, M. (2015). *Wave loads on a point-absorbing wave energy device in extreme waves.* Paper presented at the The Twenty-fifth International Ocean and Polar Engineering Conference.

Grabbe, M., Lundin, U., & Leijon, M. (2001). Ocean Energy. doi:10.1007/978-94-007-1402-1_5

Greaves, D., & Iglesias, G. (2018). *Wave and tidal energy*: Hoboken, NJ : Wiley.

Harris, M. (2018). Seabased signs deal to install 100 MW wave energy park in Ghana. Retrieved from https://www.hydroreview.com/2018/03/21/seabased-signs-deal-to-

install-100-mw-wave-energy-park-in-ghana/

Holmes, B. (2009). *Tank testing of wave energy conversion systems: marine renewable energy guides*: European Marine Energy Centre.

Holmes, B., & Nielsen, K. (2010). Guidelines for the development & testing of wave energy systems. *International Energy Agency Ocean Energy Systems*.

Hong, Y. (2016). *Numerical Modelling and Mechanical Studies on a Point Absorber Type Wave Energy Converter.* Acta Universitatis Upsaliensis,

Ingram, D. M. (2011). *Protocols for the equitable assessment of marine energy converters*: Lulu. com.

Kelly, T., Dooley, T., Campbell, J., & Ringwood, J. (2013). Comparison of the experimental and numerical results of modelling a 32-oscillating water column (OWC), V-shaped floating wave energy converter. *Energies, 6*(8), 4045-4077.

Li, Y., & Yu, Y. H. (2012). A synthesis of numerical methods for modeling wave energy converter-point absorbers. *Renewable & Sustainable Energy Reviews, 16*(6), 4352-4364. doi:10.1016/j.rser.2011.11.008

Liang, C., & Zuo, L. (2017). On the dynamics and design of a two-body wave energy converter. *Renewable energy, 101*, 265-274.

Lynn, P. A. (2014). *Electricity from wave and tide : an introduction to marine energy*: Chichester, West Sussex, United Kingdom : John Wiley & Sons Inc.

MarineEnergy. (2020). https://marineenergy.biz/2015/02/17/estimate-of-global-potential-tidal-resources/.

Misra, S. C. (2015). *Design principles of ships and marine structures*: CRC Press.

Murdock, H. E., Gibb, D., André, T., Appavou, F., Brown, A., Epp, B., . . . Ranalder, L. (2019). Renewables 2019 Global Status Report.

NikWB, W., Sulaiman, O., Rosliza, R., Prawoto, Y., & Muzathik, A. (2011). Wave energy resource assessment and review of the technologies. *Energy Environment, 2*(6), 1101-1112.

Pastor, J., & Liu, Y. (2014). Frequency and time domain modeling and power output

for a heaving point absorber wave energy converter. *International Journal of Energy Environmental Engineering, 5*(2-3), 101.

Payne, G. S., Taylor, J. R., & Ingram, D. (2009). Best practice guidelines for tank testing of wave energy converters. *The journal of ocean technology, 4*(4), 38-70.

Pecher, A., Kofoed, J. P., & SpringerLink. (2017). *Handbook of Ocean Wave Energy*: Cham : Springer International Publishing : Imprint: Springer.

Pelc, R., & Fujita, R. M. (2002). Renewable energy from the ocean. *Marine Policy, 26*(6), 471-479.

Poullikkas, A. (2014). Technology prospects of wave power systems. *Electronic Journal of Energy Environment, 2*(1), 47-69.

Robyns, B., Davigny, A., François, B., Henneton, A., & Sprooten, J. (2012). *Electricity production from renewable energies*: John Wiley & Sons.

Rusu, E., & Onea, F. (2018). A review of the technologies for wave energy extraction. *Clean Energy, 2*(1), 10-19.

Salmon, R. (2008). Introduction to ocean waves. *Scripps Institution of Oceanography, University of California, San Diego*.

Salter, S. H. (1974). Wave power. *Nature, 249*(5459), 720-724.

Seabased. (2020). https://www.seabased.com/projects.

Singiresu, S. R. (1995). *Mechanical vibrations*: Addison Wesley.

Titah-Benbouzid, H., & Benbouzid, M. (2015). An up-to-date technologies review and evaluation of wave energy converters.

Xie, J., & Zuo, L. (2013). Dynamics and control of ocean wave energy converters. *International Journal of Dynamics, 1*(3), 262-276.

Yavuz, H., McCabe, A., Aggidis, G., & Widden, M. (2006). Calculation of the performance of resonant wave energy converters in real seas. *Proceedings of the Institution of Mechanical Engineers, Part M: Journal of Engineering for the Maritime Environment, 220*(3), 117-128.

Yimin, Z. J. T. U. P., Beijing. (2007). Mechanical vibration. *3*, 480.

Yin, Y.-J. S. S., & Technology Press, S. (2013). Principle and Device of the Ocean Wave Energy Conversion Generation.

Yu, Y.-H., Li, Y., & Fluids. (2013). Reynolds-Averaged Navier–Stokes simulation of the heave performance of a two-body floating-point absorber wave energy system. *Computers, 73*, 104-114.